Noroviruses subvert the core stress granule component G3BP1 to promote viral VPg-dependent translation.

Authors:
Myra Hosmillo[1]*, Jia Lu[1]*, Michael R. McAllaster[2]*, James B. Eaglesham[1,3], Xinjie Wang[1,4], Edward Emmott[1,5], Patricia Domingues[1], Yasmin Chaudhry[1], Timothy J Fitzmaurice[1], Matthew K.H. Tung[1], Marc Panas[6], Gerald McInerney[6], Nicholas Locker[7], Craig B. Wilen[8#] and Ian Goodfellow[1#]

1. Division of Virology, Department of Pathology, University of Cambridge
2. Washington University School of Medicine, Department of Pathology and Immunology, St. Louis, MO 63110
3. Department of Microbiology, Harvard Medical School, Boston, MA 02115
4. Institute for Brain Research and Rehabilitation, South China Normal University, Guangzhou 510631, China
5. Department of Bioengineering & Barnett Institute for Chemical and Biological Analyses, Northeastern University, Boston, MA 02115
6. Department of Microbiology, Tumor and Cell Biology, Karolinska Institute, Stockholm, Sweden
7. School of Biosciences and Medicine, University of Surrey, Guildford UK.
8. Yale School of Medicine, Departments of Laboratory Medicine and Immunobiology, New Haven, CT 06520

* These authors contributed equally to the work
# Corresponding authors:
Craig B Willen: craig.wilen@yale.edu
Ian Goodfellow: ig299@cam.ac.uk

Abstract (133)

Knowledge of the host factors required for norovirus replication has been hindered by the challenges associated with culturing human noroviruses. We have combined proteomic analysis of the viral translation and replication complexes with a CRISPR screen, to identify host factors required for norovirus infection. The core stress granule component G3BP1 was identified as a host factor essential for efficient human and murine norovirus infection, demonstrating a conserved function across the *Norovirus* genus. Furthermore, we show that G3BP1 functions in the novel paradigm of viral VPg-dependent translation initiation, contributing to the assembly of translation complexes on the VPg-linked viral positive sense RNA genome by facilitating ribosome recruitment. Our data uncovers a novel function for G3BP1 in the life cycle of positive sense RNA viruses and identifies the first host factor with pan-norovirus pro-viral activity.

Keywords (10)

Norovirus, stress granule, G3BP1, CRISPR, replication complex, calicivirus, proteomics.

Introduction:

Positive sense RNA viruses rely heavily on host cell factors for all aspects of their life cycle. They replicate on host derived membranous vesicles that are induced following viral infection, the formation of which requires the activity of key membrane bound viral enzymes (Altan-Bonnet, 2017). Within the membrane bound viral replication complex, translation of the viral genome and the synthesis of new viral RNA occurs in a highly coordinated process. Positive sense RNA viruses have evolved novel gene expression mechanisms that enable them to overcome the genome size limitations that accompany error-prone replication and which might restrict their overall coding capacity (Firth and Brierley, 2012). In addition, viral modification of the host cell translation machinery often provides a competitive advantage allowing for the efficient translation of viral RNA in an environment where competing cellular RNAs are in abundance (McCormick and Khaperskyy, 2017). This ability to compete with cellular RNAs is particularly important for the initiation of infection where the incoming viral genome may be present at only a single copy per cell.

We have previously described a novel paradigm of viral translation that relies on the interaction of host translation initiation factors with a virus-encoded protein (VPg), covalently linked to the 5’ end of the genome of members of the *Caliciviridae* family of positive sense RNA viruses (Chaudhry et al., 2006; Chung et al., 2014; Goodfellow et al., 2005; Hosmillo et al., 2014; Leen et al., 2016). Unlike the 22-amino acid VPg peptides from picornaviruses, the VPg protein linked to the genomes of caliciviruses is significantly larger and is essential for the translation of viral RNA and viral RNA infectivity (Goodfellow, 2011).

Human noroviruses (HuNoV) and sapoviruses (HuSaV) are enteropathogenic members of the *Caliciviridae* family of positive sense RNA viruses, and together cause >20% of all cases of gastroenteritis (GE). They are also a significant cause of morbidity and mortality in the immunocompromised; individuals with genetic immune-deficiencies, cancer patients undergoing treatment and transplant recipients often experience chronic norovirus infections lasting months to years (van Beek et al., 2016). The economic impact of HuNoV is estimated to be at least ~$4.2 billion in direct health care costs, with wider societal costs of ~$60 billion (Bartsch et al., 2016). Despite their socioeconomic impact, we have, until very recently lacked a detailed understanding of much of the norovirus life cycle and many significant questions remain unanswered. HuNoV replicons (Chang et al., 2006), a murine norovirus that replicates in cell culture (Karst et al., 2003; Wobus et al., 2004) and the recent B cell (Jones et al., 2014), stem-cell derived organoid (Ettayebi et al., 2016) and zebrafish larvae infection models (Van et al., 2019), have all provided invaluable tools to dissect the norovirus life cycle. However, due to the technical limitations associated with many of these experimental systems, in comparison to other positive sense RNA viruses, our knowledge of the intracellular life of noroviruses is significantly lacking (reviewed in Thorne and Goodfellow, 2014).

In the current study, we have combined three independent unbiased approaches to identify host factors involved in the norovirus life cycle. Combining experimental systems that incorporated both murine and human noroviruses, allowed the identification of cellular factors for which the function is likely conserved across the *Norovirus* genus. By combining three complimentary approaches, we identify the

host protein G3BP1 as a critical host factor required for norovirus VPg-dependent translation, identifying a new role for G3BP1 in virus-specific translation.

Results:

Comparative analysis of the norovirus translation initiation complex.

The MNV and the prototype HuNoV Norwalk virus (NV) VPg proteins are covalently linked to the viral genome via the highly conserved tyrosine residue within an N-terminal DEEYD/E motif found in all calicivirus VPg proteins (Figure 1A). In addition, the norovirus VPg proteins contain a highly conserved C-terminal domain which we have shown to be necessary and sufficient for binding to the translation initiation factor eIF4G via an interaction that requires a highly conserved phenylalanine residue (Figure 1A) (Chung et al., 2014; Leen et al., 2016). Using affinity purification on m7-GTP sepharose, we confirmed that the NV VPg protein, as produced during authentic virus replication in a NV replicon bearing cell line, interacts with the cap-binding complex eIF4F (Figure 1B). Components of the eIF4F complex, namely the eIF4E cap-binding protein, the eIF4A helicase and the eIF4GI scaffold protein, along with poly-A binding protein (PABP) and eIF3 subunits, were readily purified on m7-GTP sepharose, whereas GAPDH was not. In NV-replicon containing cells, mature VPg was also enriched on m7-GTP sepharose but the NS3 protein, known to have RNA binding and helicase activity (Li et al., 2018), was not. Furthermore, we demonstrated that transfection of GFP-tagged versions of either the MNV or NV VPg proteins into 293T cells allowed for the affinity purification of eIF4F components and that mutations in the eIF4G binding domain of VPg reduced this association (Figure 1C).

We next used quantitative mass spectrometry of the affinity purified complexes isolated from cells transfected with the GFP-Tagged VPg proteins to identify host factors specifically enriched on the norovirus VPg protein (Figure 1D, Figure 1-figure supplement 1 and Supplementary file 1). Most of the proteins identified were components of the host cell translation complex including ribosomal proteins, translation initiation factors and host RNA binding proteins. These data agrees with but significantly extend our previous observations using a less sensitive multi-step affinity purification approach to characterise host factors associated with the MNV VPg protein only (Chaudhry et al., 2006; Chung et al., 2014). In addition, we identified hnRNPA1 which we have previously shown to act in norovirus genome circularization (López-Manríquez et al., 2013). YBX1, DDX3 and several other proteins that we have previously found to interact with the 5' end of the viral RNA (Vashist et al., 2012b) were also enriched on VPg (Figure 1-figure supplement1). To validate a select number of these interactions and to assess whether the interaction of VPg with eIF4G is required for their association with VPg, we performed western blot analysis of complexes purified from cells transfected with either the WT or eIF4G-binding mutants (Figure 1E). Except for YBX1, the association of all proteins tested were reduced by the introduction of eIF4G-binding site mutations into the MNV VPg protein. Together, these data extend our previous observations and confirm that the norovirus VPg proteins interact with a complex network of host factors, many of which have been implicated in the host cell translation initiation process.

Determination of the norovirus replication complex proteome.

To further identify the components of the norovirus translation and replication complex, as formed during authentic viral replication in highly permissive cells, we utilised two recombinant infectious MNV strains that carried epitope purification tags within the NS1/2 or NS4 proteins (McCune et al., 2017) (Figure 2A). The insertion positions were previously identified using a transposon based mutagenesis screen as sites that tolerate insertions, without compromising virus viability (Thorne et al., 2012). Our approach was somewhat analogous to that recently published for coronaviruses (V'kovski et al., 2019) but instead used stable isotope labelling of permissive cells and the FLAG affinity purification tag rather than proximity labelling. Unlabelled or stable isotope labelled highly permissive BV2 microglial cells were infected with either wild type MNV or the equivalent virus carrying the FLAG epitope purification tag in either NS1/2 or NS4, and the viral replication complex was purified. The experiment was performed three times by swapping the labelled derivatives of arginine and lysine as described in the materials and methods. Silver stain of the purified complexes confirmed the presence of the bait proteins, with both the uncleaved and cleaved forms of NS1/2 and NS2 being highly enriched (Figure 2B). As expected, complexes purified from NS1/2-Flag virus infected cells co-purified untagged NS4 and vice versa (Figure 2B), as we have previously shown these proteins to interact to form a complex (Thorne et al., 2012). Western blot analysis of the purified complexes confirmed that viral non-structural and structural proteins were specifically enriched in the purified complexes, including NS5 (VPg)-containing precursors (Figure 2C). We noted that anti-NS4 monoclonal antibody was unable to detect protein in the extracts prior to enrichment, which most likely reflected the limited sensitivity of the antibody. Quantitative mass spectrometry of the purified

complexes allowed the identified of viral and cellular proteins enriched in the complex (Figure 2D and Supplementary file 2).

As expected, all viral proteins, including the VF1 protein product of ORF4, an innate immune antagonist (Bailey et al., 2011), were enriched in the viral replication complex. There was a significant correlation between the relative enrichment of proteins identified using NS1/2 and NS4 (Spearman correlation of 0.8832), fitting with our prior knowledge that both proteins form a complex during viral replication (Thorne et al., 2012). Ontology analysis indicated that proteins involved in vesicle transport and fatty acid metabolism were significantly enriched (Figure 2-figure supplement 1 and Supplementary file 3), fitting with previous observations that the viral replication complex is associated with cytoplasmic membranous structures (Cotton et al., 2017; Hyde and Mackenzie, 2010; Hyde et al., 2009). Several host proteins previously identified in a variety of biochemical and genetic screens were enriched (Figure 2-figure supplement1 and Supplementary file 3) providing additional confidence that the approach identified biologically relevant interactions. We noted that the VapA and the paralogue VapB, which we have recently identified as binding to the NS1/2 protein (McCune et al., 2017), were both highly enriched.

We observed that NS4 failed to enrich mature VPg, instead purifying only the polyprotein cleavage intermediate NS4/5(VPg) (Figure 2C & S2.2). In contrast, NS1/2 effectively pulled down mature VPg (Figure 2C & S2.2). Consistent with this, NS1/2 enriched the VPg binding partner eIF4G more than 2-fold, while pulldown of NS4 resulted in no eIF4G enrichment, likely indicating that the NS4/5 (VPg) precursor cannot effectively function in translation initiation (Figure 2-figure supplement 2). This is consistent with a previous observation that binding of C-

terminal VPg fusion proteins to eIF4G is inhibited {Leen:2016gt}, but may further suggest that the function of VPg is also altered when present as an N-terminal fusion with NS4. Comparison with the proteomics data obtained using VPg as a bait protein (Figure 1) showed some degree of overlap with our replication complex proteome data (Figure 2-figure supplement 2). Consistent with our observations with the well-established VPg partner eIF4G, most host factors identified using VPg were enriched by >2-fold using only the NS1/2 tagged virus, and not the NS4-tagged virus. Ontology analysis of host factors enriched by both VPg and NS1/2 more than 2-fold reveals a cross-section of the replication complex proteome dedicated to translation, and RNA metabolism (Figure 2-figure supplement 2 and Supplementary file 3). One protein was enriched by VPg, NS1/2, and NS4 – the core stress granule protein G3BP1 (Figure 2-figure supplement 2).

Identification of host factors required for norovirus infection using a CRISPR-knockout screen.

A high density CRISPR library screen was undertaken to identify genes that contribute to the norovirus life cycle. The Brie library (Doench et al., 2016) was selected due to the reduced off-target effects relative to previously described CRISPR libraries used for norovirus studies (Haga et al., 2016; Orchard et al., 2016). In addition, to minimise the impact of gRNAs that may have deleterious effects on long term cell viability and to increase our ability to detect genes that may be important, but not essential, for norovirus-induced cell death, the infection was reduced to 24 hours as compared to 2-10 days post infection in previous studies. BV2-Cas9 expressing cells were infected with lentiviruses carrying the Brie gRNA

library carrying 78,637 independent guide RNAs to 19,674 genes (Doench et al., 2016). The transduced cells were then infected with two MNV strains, CW3 and CR6, which cause acute and persistent infections in immunocompetent mice respectively (Nice et al., 2012; Thackray et al., 2007), and guide RNA abundance compared to mock infected cells at 24 hours post infection as illustrated in Figure 3A. Genes that were enriched by STARS analysis following MNV infection represent putative pro-viral factors which when disrupted, resulting in slower cell death, whereas those with a negative STARS value represent putative anti-viral factors where virus-induced cell death has occurred quicker, resulting in their underrepresentation in the final pool of cells. MNV-CR6 infection resulted in 212 genes being enriched and 42 being negatively selected (Figure 3B), whereas for MNV-CW3 279 and 18 genes were positively and negatively selected respectively (Figure 3B). In most cases, there was a clear correlation between the datasets obtained using either strain (Figure 3C). STARS analysis was used to ranks genes with positive and negative values with an FDR value less than 0.05 (Supplementary file 4). In both screens, the MNV receptor Cd300lf was the most highly positively selected gene identified, in agreement with previous reports (Haga et al., 2016; Orchard et al., 2016). The previously characterised pro-viral MNV gene VapA (McCune et al., 2017) was also identified in both screens (Supplementary file 4). The second most highly enriched gene was G3BP1, a gene also identified in one of the two previous CRISPR screens performed on norovirus infected cells (Orchard et al., 2016).

Comparing the CRISPR data obtained in this study using two divergent strains of MNV showed a high degree of overlap, with 89 common pro-viral hit and 5 common anti-viral hits (Supplementary file 4). However comparison with the previous reported

CRISPR screen used to identify the MNV receptor (Orchard et al., 2016) showed only 7 proviral hits for CW3 and 8 for CR6, of which only 4 were common for both strains across all screens (Supplementary file 4). The 4 genes identified were the MNV receptor CD300lf, the stress granule component G3BP1, the histone methytransferase Kmt2d and Smarce1, which encodes an actin dependent regulator of chromatin. The discrepancy between the screens performed here and those in previous studies likely reflects the experimental conditions under which the screens were undertaken i.e. 24 hours of infection vs 2-3 days in the previous screens. The previous screen was performed under much more stringent conditions that were unlikely to identify proteins that play a role in the norovirus life cycle but are not essential. Pathway over-representation analysis {Liao:2019fn} of the genes pro-viral genes identified in the CRISPR screens performed in this study highlighted mRNA processing, RNA splicing and methylation as the three most highly represented gene ontology (GO) terms (Supplementary file 4). The gene encoding PTBP1, polypyrimidine tract binding protein, was one of the genes identified in these enriched GO terms. PTBP1 is a protein we have previously shown to bind to a 3' pyrimidine-rich stretch in the MNV genome which is important for viral pathogenesis {Bailey:2010fz}. The interaction of PTBP1 with the viral 3' end also facilitates the recruitment of PTBP1 to the viral replication complex where it contributes to an as yet undefined aspect of the norovirus life cycle {Vashist:2012ke}.

A cross-comparison of the data obtained from all three approaches allowed us to identify several host proteins that were common to all screens (Supplementary file 5). G3BP1, the core stress granule component was identified in all three screens as a potential host factor essential for norovirus infection. G3BP1 was found to be associated with the MNV and NV VPg proteins (Figure 1D), enriched in viral

replication complexes purified using either NS1/2 or NS4 flag tagged viruses (Figure 2D) and identified in a CRISPR screen using two different MNV strains as a putative pro-viral factor involved in the norovirus life cycle (Figure 3C).

G3BP1 is essential for murine norovirus replication

To validate the importance of G3BP1 in the norovirus life cycle we generated G3BP1 deficient BV2 cell lines (Figure 4A) and examined the impact of G3BP1 ablation on MNV infection. Western blotting confirmed the loss of G3BP1 in the three lines tested and we noted that at in some cases, a concomitant increase in G3BP2 expression was observed as has been previously noted (Kedersha et al., 2016). A clear defect was observed in the ability to replicate to produce infectious virus in three independently selected ΔG3BP1 cell lines (Figure 4B). This effect was mirrored by an inability to induce cytopathic effect leading to virus-induced cell death (Figure 4C&D). In contrast, the ability of encephalomyocarditis virus (EMCV) to infect and cause cell death was unaffected by the deletion of G3BP1(Figure 4C&D). These data confirm that cells lacking G3BP1 are highly resistant to norovirus infection.

G3BP1 is essential for human norovirus replication in cell culture

To determine if the G3BP1 was also essential for HuNoV, we examined the impact of loss of G3BP1 on human norovirus replication in cell culture using the Norwalk virus replicon. To establish the experimental system, we first confirmed that the presence of VPg on the 5’ end of the Norwalk RNA was essential for the replication

of the replicon RNA and for the capacity to form G418 resistant colonies. Transfection of replicon RNA, purified from replicon containing cells, into BHK cells readily resulted in the formation of antibiotic resistant cell colonies (Figure 5A). In contrast, RNA that was proteinase K treated prior to transfection was unable to produce replicon containing colonies. Transfection of replicon RNA into wild type U2OS osteosarcoma cells allowed the formation of replicon-containing colonies, although the efficiency of formation was significantly less than that seen in BHK cells (Figure 5B). CRISPR modified U2OS cells that lacked G3BP1 (Kedersha et al., 2016) were unable to support NV replication, as evident by the lack of antibiotic resistant colonies (Figure 5B). To further examine the role of G3BP1 in human Norwalk virus replication, WT or G3BP1 deficient U2OS cells were transfected with NV replicon VPg-linked RNA, and RNA synthesis monitored overtime following the addition of G418. While a significant increase in NV viral RNA levels was seen in WT U2OS cells, those lacking G3BP1 were completely unable to support NV RNA synthesis (Figure 5C). We further validated these observations by transfection of the NV replicon in murine BV2 microglial cells which were able to support HuNoV replication by the formation of small microcolonies of antibiotic resistant cells (Figure 5D). In the absence of G3BP1 the formation of antibiotic resistant microcolonies was completely ablated and then subsequently restored in ΔG3BP1 cells engineered to express the wild type version of G3BP1 (Figure 5D). These data indicate that like for MNV, G3BP1 is essential for human Norwalk virus replication.

The RNA-binding domain of G3BP1 is required for its function in the norovirus life cycle.

To confirm the role of G3BP1 in the norovirus life cycle we examined the ability of full length and truncated versions of G3BP1 to restore norovirus replication in G3BP1 knockout cells. A mouse BV2 G3BP1 knockout cell line was complemented with either full length G3BP1 or variants lacking the RGG or both the RGG and RRM binding domains (Figure 6A) and the impact on viral replication assessed. Complementation with full length murine G3BP1 restored the ability of MNV to induce cell death (Figure 6B) and to produce infectious virus (Figure 6C) back to near wild type levels. In contrast, complementation with a variant carrying a deletion of the RGG domain resulted in limited complementation, and deletion of both the RGG and RRM domains together resulted in complete loss of complementation capacity (Figure 6B&C). These data confirm that the RNA binding domains of G3BP1 are essential for its function in the norovirus life cycle.

To further define the role of G3BP1 in the norovirus life cycle and to confirm that the function of G3BP1 was downstream of virus binding and viral entry, we therefore bypassed the entry phase of the infection process and transfected MNV VPg-linked RNA into WT and two independently generated BV2 ΔG3BP1 cell lines and examined the impact on norovirus replication. Transfection of MNV viral VPg-linked RNA into WT cells resulted in high yields of infectious virus (Figure 7A) and viral proteins (Figure 7C). The levels of infectivity obtained following transfection of ΔG3BP1 cell lines with MNV viral RNA was comparable to that obtained in WT cells in the presence of the nucleoside analogue 2'-C-methylcytidin (2CMC), a known inhibitor of the norovirus RNA polymerase (Rocha-Pereira et al., 2012; 2013) (Figure 7A). No viral proteins were detected in either of the ΔG3BP1 cell lines suggesting a defect at a very early stage in the viral life cycle (Figure 7C). Transfection of VPg-linked RNA into the ΔG3BP1 cell lines reconstituted with WT G3BP1 restored the

342 ability to produce infectious virus (Figure 7B) and the production of viral proteins
343 (Figure 7D). A minor increase in viral infectivity was observed in the ΔG3BP1 cell line
344 reconstituted with the ΔRGG construct producing viral titres that were higher than
345 those obtained from the WT complemented line in the presence of 2CMC,
346 suggesting low levels of viral replication (Figure 7B). However, the levels of viral
347 proteins produced in this line was below the limit of detection by western blot (Figure
348 7D). These data confirm that G3BP1 is required for a post entry stage of the
349 norovirus life cycle and that in the absence of G3BP1 no norovirus replication was
350 observed within the sensitivity of the assay used.

351

352 **G3BP1 is required for, or prior to, viral negative strand RNA synthesis**

353 To define the precise role of G3BP1 in the early stages of the virus life cycle, we
354 used strand-specific RT-qPCR to quantify the levels of viral positive and negative
355 sense RNA in WT and ΔG3BP1 cell lines following infection with MNV. As a control,
356 2CMC was included following virus inoculation as illustrated in the experimental time
357 line (Figure 8A). The production of viral positive sense RNA was reduced to
358 background levels in the absence of G3BP1, comparable to levels observed when
359 the 2CMC was present during the infection (Figure 8B). Viral negative sense RNA
360 synthesis was also reduced to below the detection limit of the assay in ΔG3BP1 cell
361 lines (Figure 8C). Surprisingly, we were able to detect an ~5 fold increase in viral
362 negative sense RNA production at 6 hours post infection of WT cells in the presence
363 of 2CMC, which, given that 2CMC was added after the inoculation phase (Figure
364 8B), likely represents the first round of viral negative sense RNA synthesis,

365 confirming the sensitivity of the assay. Addition of 2CMC during the inoculation
366 phase reduced this background levels (data not shown).

367 Similar results were obtained following transfection of viral RNA into cells to bypass
368 the entry phase; viral positive and negative sense RNA synthesis was near (or
369 below) the sensitivity of the assay following transfection of viral VPg-linked RNA into
370 two independent ΔG3BP1 cell lines (Figure 8D & E). Complementation with WT
371 G3BP1, but not the mutant forms lacking the RNA binding domains, also restored
372 viral positive and negative sense RNA synthesis (Figure 8F & G). We did not detect
373 viral positive or negative sense RNAs in the ΔRGG complemented cell line, despite
374 the presence of low levels of viral infectivity (Figure 7B). This discrepancy likely
375 reflects the relative sensitivities of the assays and the nature of the strand specific
376 qPCR assay which requires low levels of RNA input to maintain strand specificity.
377 Together these data suggest that the function of G3BP1 is prior to, or at the level of
378 viral negative sense RNA synthesis, with the most logical steps being either viral
379 RNA translation or the formation of viral replication complexes.

380

381 **G3BP1 is required for the association of VPg with ribosomal proteins.**

382 We have previously shown that norovirus VPg interacts with eIF4G to recruit
383 ribosomal subunits and direct viral translation (Chaudhry et al., 2006; Chung et al.,
384 2014). The interaction between VPg and eIF4G occurs via a direct interaction
385 between the highly conserved C-terminal region in VPg and the central HEAT
386 domain of eIF4G (Leen et al., 2016) and does not require any additional cellular
387 cofactors, as a stable complex can be formed between VPg and the eIF4G HEAT

388 domain at least *in vitro*. The interaction between the eIF4G HEAT domain and the
389 eIF3 complex plays a central role in the recruitment of the 40S ribosomal subunit for
390 translation initiation (Marcotrigiano:2001uq; Kumar et al., 2016; Villa et al., 2013).
391 Our proteomics analysis also confirms that the norovirus VPg proteins form a
392 complex that contains multiple components of the large and small ribosomal subunits
393 (Figure 1D). It has been established previously that G3BP1 associates with 40S
394 subunits (Kedersha et al., 2016). To assess a potential role for G3BP1 in the
395 formation of VPg-driven translation complexes in cells, we examined the ability of
396 GFP tagged versions of MNV VPg to pull down ribosomal proteins in the presence
397 and absence of G3BP1. GFP-tagged WT MNV VPg was readily able to pull down
398 eIF4G, G3BP1 and RpS6, a component of the 40S subunit (Figure 9A). However, in
399 the absence of G3BP1, the ability to pull down RpS6 and RpS3 was lost (Figure 9A
400 and Figure 9-figure supplement 1). Furthermore, we found that disruption of the VPg-
401 eIF4G interaction by the introduction of the F123A mutation into the eIF4G binding
402 domain, also significantly reduced the ability to pull down RpS6, RpS3, as well as
403 RpL4, a component of the large ribosomal subunit (Figure 9B and Figure 9-figure
404 supplement 1). We also observed that upon reconstitution of G3BP1 expression, the
405 levels of RpS6, RpS3 and RpL4 associated with VPg were enhanced (Figure 9B and
406 Figure 9-figure supplement 1). We note however that the levels of ribosomal proteins
407 associated with the GFP-tagged VPg in this assay is relatively low, we think this
408 reflect the fact that in the context of viral infection where VPg is covalently linked to
409 viral RNA, secondary interactions between translation initiation factors and the viral
410 RNA likely stabilise this complex. We have previously seen that the eIF4A protein
411 binds directly to the 5' end of the sapovirus genome {Hosmillo:2016fp}. Furthermore,
412 eIF4G is known to make secondary stabilising interactions with the template RNA

that are critical for translation initiation {Yanagiya:2009fm}. Therefore we hypothesise that in the absence of covalently linked viral RNA, the association of VPg with ribosomal subunits is less robust and therefore less able to be maintained during the purification process used in the GFP-Trap approach. Therefore, to assess how the loss of G3BP1 may influence the association of VPg-linked viral RNA with ribosomal subunits in a more physiologically relevant system, we quantified the amount of viral VPg-linked RNA bound to ribosomal subunits by RNA-IP. By inclusion of the viral RNA polymerase inhibitor 2CMC we were able to assess viral RNA association with ribosomal proteins in the absence of viral RNA synthesis. We found that in the absence of G3BP1, the amount of viral RNA associated with the ribosomal subunit protein RpS3 was decreased (Figure 9C). These data suggest that that G3BP1 likely contributes in some manner to the association of VPg and viral VPg-linked RNA with ribosomal subunits.

G3BP1 is required for efficient polysome loading of norovirus VPg-linked RNA

To assess the impact of G3BP on the translation of viral VPg-linked RNA following viral infection, we evaluated the impact of loss of G3BP1 on the recruitment of viral RNA to polysomes under conditions where viral RNA synthesis was inhibited, namely in the presence of 2CMC. This approach enabled us to assess only the capacity of the incoming parental viral RNA to assemble into translationally active complexes, a stage often referred to as the “maiden round” of RNA virus genome translation. To this aim, cells were infected with MNV in the presence of 2CMC and polysomes profiling on extracts prepared from cells at 4 and 9 hours post infection performed (Figure 10A). Quantification of the viral RNA levels in cells in the

presence of 2CMC confirmed that the absence of G3BP1 has no impact on the overall levels present at the time points examined (data not shown). We noted that even in the presence of 2CMC, which inhibits viral RNA synthesis, there was a small but measurable increase in free 80S ribosomes over time in WT cells but not in cells lacking G3BP1 (Figure 10A). We have previously found that MNV infection results in translation shut off and that this effect is at least partially due to the activity of the NS6 protease (Emmott et al., 2017). The fact we observed 80S accumulation in WT cells, even in the absence of viral RNA synthesis, but not in cells lacking G3BP1, indirectly lead us to suspect that translation of viral RNA had occurred in WT cells, but was much less efficient in cells lacking G3BP1. Further analyses indicated that while most ribosome-associated norovirus RNA in WT cells was found in polysomes containing fractions, less viral RNA was found in ribosome-containing fractions (1-12 in Figure 10A & B) in the absence of G3BP1 and, in comparison to WT cells, very little viral RNA was found in fractions containing polysomes (Figure 10B). Extending the fractionation to include the free RNA and ribonucleoprotein complexes at the top of each gradient confirmed that in the absence of G3BP1 norovirus RNA is less efficient at assembling into polysomal fractions, suggesting a defect at the level of viral protein synthesis (Figure 10C). Together these data support the hypothesis that G3BP1 functions to promote the translation of norovirus VPg-linked RNA, by facilitating the association with ribosomal subunits and the formation of polysomes on viral RNA.

G3BP1 is require for efficient norovirus VPg-dependent translation.

To further examine a potential role of G3BP1 in norovirus VPg-dependent translation, cytoplasmic translationally competent extracts were prepared from WT and ΔG3BP1 cell lines. In order to ensure comparable overall translation efficiencies between extracts, RNA generated from a cricket paralysis virus IRES (CrPV) bicistronic reporter plasmid (a kind gift from Professor Ian Brierley, University of Cambridge) was used to measure cap-dependent and cap-independent translation {Wang:2013kh}. The dual luciferase construct was *in vitro* transcribed, capped and poly(A) tailed. Renilla luciferase was produced via cap-dependent translation initiation whilst firefly luciferase was synthesised via cap-independent, CrPV IRES-dependent translation (Figure 11A). Both cap-dependent (Figure 11B) and CrPV IRES-dependent translation (Figure 11C) were comparable in extracts prepared from WT and ΔG3BP1 cell lines (Figure 11A). To compare norovirus VPg-dependent translation efficiency between WT and ΔG3BP1 lysates, viral VPg-linked RNA was first extracted from sucrose cushion-purified MNV virions and the presence of VPg on the viral RNA 5' end confirmed by resistance to XrnI mediated degradation *in vitro* (Figure 11-figure supplement 1 panel A). The translation profile of the purified viral RNA was further analysed by translation in rabbit reticulocyte lysates in comparison to *in vitro* transcribed viral genomic and sub-genomic RNAs (Figure 11-figure supplement 1 panel B). We found that norovirus VPg-dependent translation was reduced in nuclease treated extracts prepared from cells lacking G3BP (Figure 11D). Quantification of the levels of multiple viral proteins produced over multiple experiments indicated that translation in nuclease treated extracts was on average reduced by ~40-50% because of G3BP1 ablation (Figure 11E). A similar reduction in *in vitro* translation was observed across multiple time points (Figure 11-figure supplement 1 panel C). This 50% reduction in translation efficiency was also

485 consistently observed in extracts that were not nuclease treated, and therefore
486 contained physiologically relevant levels of cellular mRNAs (Figure 11F & G). These
487 data further confirm that G3BP1 functions to enhance norovirus VPg-dependent
488 translation initiation.

489

490 **Discussion**

491 In this study, we have used a combination of biochemical and genetic approaches to
492 identify host factors involved in the norovirus life cycle. Our combined approaches
493 resulted in the identification of the core stress granule component G3BP1 as a host
494 protein critical for the replication of both murine and human noroviruses in cell
495 culture. Furthermore, we determined that G3BP1 plays a key role in the processes of
496 norovirus VPg-dependent protein synthesis, uncovering a new function for G3BP1 in
497 facilitating RNA virus genome translation.

498 The orthogonal approaches used in the current study provide an unprecedented
499 insight into the identity of host factors with potential roles in the norovirus life cycle.
500 The detailed proteomic analysis of the viral replication and translation complexes
501 formed during MNV infection (Figure 2) resulted in the identification of several host
502 factors with previously identified roles in the MNV life cycle. We focused our efforts
503 on G3BP1 as it was identified in all three approaches and was also identified in a
504 CRISPR screen published during this study (Orchard et al., 2016). Furthermore, we
505 have previously shown that feline calicivirus (FCV), a relative of noroviruses within
506 the *Vesivirus* genus, cleaves G3BP1 to inhibit stress granule formation (Humoud et
507 al., 2016). In contrast, MNV infection does not result in G3BP1 cleavage and instead

forms cytoplasmic foci the composition of which is distinct from canonical stress granules (Brocard et al., 2018).

G3BP1 is one member of a group of G3BP proteins (Ras-GTPase-activating protein (SH3 domain)-binding proteins), referred to as Rasputin in insects, that possess RNA binding activity and have multiple cellular functions including the regulation of RNA stability and translation in response to stress. Originally identified as a protein that interacted with Ras-GTPase activating protein (RasGAP), more than two decades of research have significantly expanded our knowledge of the multifunctional role in cellular processes. It is now well accepted that G3BPs play a role in cancer cell survival, cancer metastasis and invasion, processing of specific miRNAs and stress granule formation (Reviewed in (Alam and Kennedy, 2019). Stress granules are dynamic cytoplasmic ribonucleoprotein complexes that form rapidly under stress conditions and within which cellular RNAs are stored in stalled translation complexes (Protter and Parker, 2016). In the context of viral infection, numerous studies have suggested that many, if not all, viruses must interact in some manner with stress granules as there is growing evidence that the formation of cytoplasmic stress granules is part of the anti-viral defence mechanism (Reviewed in (McCormick and Khaperskyy, 2017). Some viruses interact with stress granules to promote viral replication (Cristea et al., 2010; Kim et al., 2016; Panas et al., 2014; 2012) whereas some do so to counteract the inhibitory effect of stress granules on the translation of viral RNA (Panas et al., 2015; White et al., 2007).

Our data suggests that G3BP1 plays a key role in promoting the translation of norovirus VPg-linked viral RNA. Positive sense RNA viruses have evolved mechanisms to ensure the efficient translation of their viral genomic RNAs in the

presence of high concentrations of competing cellular RNAs. These mechanisms include the use of internal ribosome entry site elements (IRES), modified cap-dependent mechanisms (Firth and Brierley, 2012; Jaafar and Kieft, 2019) and the ability to target the host cell translation machinery to generate an environment where viral RNA translation is favoured over cellular capped RNAs (Walsh et al., 2013). G3BP1 is thought to associate primarily with free 40S subunits (Kedersha et al., 2016). Our data supports a hypothesis whereby the association of G3BP1 with 40S ribosomal subunits somehow stabilises the recruitment of a translation initiation complex to the 5' end of the VPg-linked viral RNA genome, promoting VPg-dependent translation and thereby uncovering a new function in virus specific translation. The mechanism by which G3BP1 contributes to this process has yet to be fully explored but our data supports the hypothesis that G3BP1 directly or indirectly promotes the recruitment of ribosomal subunits to VPg-driven translation complexes. The RGG motif of G3BP1 is known to be essential for the association between G3BP1 and 40S subunits as well as the ability to from stress granules, whereas data would suggest that the RRM may play a regulatory role (Kedersha et al., 2016). These domains were also required for the function of G3BP1 in the norovirus life cycle (Figure 6) confirming that the G3BP1 association with 40S is important for its role in promoting norovirus VPg-dependent translation. Importantly, RGG domains are known to have many functions (Thandapani et al., 2013) and therefore in the context of G3BP1 function in the norovirus life cycle, may also contribute to unknown interactions that promote norovirus translation. Previous work on alphaviruses have shown that G3BP1 is sequestered by binding to the nsP3 protein (Panas et al., 2012; 2014; 2015). Furthermore, this interaction occurs via an FGDF motif also found in other viral proteins including the ICP8 protein of herpes

simplex virus (Panas et al., 2015). While the MNV VPg protein has a similar motif FGDGF (Figure 1A), this motif is not conserved in the GI Norwalk virus VPg protein. Therefore, our data suggest that the interaction of VPg with G3BP1 is not direct, fitting with our observation that this interaction is reduced by mutations in the eIF4G binding domain (Figure 1A and Figure 9B.) While our data fit with a primary role for G3BP1 in norovirus translation, we are unable to exclude the possibility that G3BP1 plays other roles in the viral life cycle. Recent studies have confirmed that G3BP1 is enriched at sites of viral RNA synthesis (Brocard et al., 2018; Fritzlar et al., 2019) so it is possible that G3BP1 makes multiple contacts between the 40S subunit and viral RNA genome directly. These additional contacts, may further promote viral VPg-dependent translation and/or another aspect of the viral life cycle.

The technical challenges associated with studying human norovirus replication in cell culture have limited the experimental approaches we could use to validate the role of G3BP1 in human norovirus translation. However, our results have clearly demonstrated that in the absence of G3BP1, human Norwalk virus is unable to replicate or form replicon-containing colonies. Furthermore we were able to show that BV2 murine microglial cells support the replication of the HuNoV GI replicon, albeit it to a lesser degree than BHK or U20S cells (Figure 5). These data confirm that all the machinery necessary for HuNoV replication is conserved between human, hamster and mouse cells. Furthermore, reconstitution of the ΔG3BP1 BV2 microglial cells with WT G3BP1, at least partially restored the ability of the HuNoV GI replicon to form colonies, confirming the specificity of the effect. The presence of G3BP1 in the NV VPg-containing complexes again fits with our hypothesis that G3BP1 plays a role in promoting viral VPg-dependent protein synthesis.

We have previously found that norovirus infection leads to preferential viral-translation whereby cellular mRNAs induced in response to norovirus infection are inefficiently translated (Emmott et al., 2017). This modification of host cell translation is at least partially driven by the ability of the viral NS6 protease to cleave PABP and the induction of apoptosis which results in cleavage of cellular translation initiation factors (Emmott et al., 2017). Importantly, whilst caspase cleaved translation initiation factors do not support host cell cap-dependent translation, we have previously found that the cleaved forms of eIF4G do support norovirus VPg-dependent translation (Emmott et al., 2017). The ability of the norovirus protease to cleave PABP and other substrates is also controlled by polyprotein processing and interactions with other viral proteins (Emmott et al., 2019). Recent work confirms that the preferential viral translation is not driven by the GCN2-mediated phosphorylation of eIF2α in MNV infected cells (Brocard et al., 2018). We note however that others have suggested that NS3 may contribute to the translational shut off seen in MNV infected cells (Fritzlar et al., 2019), with the caveat that this observation was made outside of the context of infected cells and used overexpressed tagged viral proteins. We suspect that noroviruses use multiple mechanisms that work co-operatively to enable the control of host gene expression and the subsequent translation of the cellular mRNAs. The relative contribution of these processes in any given cell type may also vary dependent on the degree to which the cells can sense and respond to viral infection through the induction of innate and apoptotic responses.

The observation that many of the factors enriched using the VPg protein were only enriched on complexes purified with NS1/2 tagged infectious MNV, could suggest that the viral proteins present in the viral translation complex are distinct from those present in complexes active for viral RNA synthesis. However, we cannot formally

606 rule out other possible explanations including the possibility that the specific
607 enrichment of translation factors on NS1/2 occurs because NS1/2 is the first protein
608 to be translated from ORF1, therefore unprocessed NS1/2 at the N-terminus of the
609 ORF1 polyprotein being actively translated could function as an anchor, facilitating
610 the enrichment of ribosomes and the associated factors. In addition, we have
611 previously seen that VPg-containing precursors may bind the translation initiation
612 factor eIF4G less well (Leen et al., 2016), which could prevent some VPg (NS5)
613 containing precursors associating with translation initiation complexes. Furthermore,
614 the norovirus replication complex contains a number of highly conserved viral
615 protein-viral protein interactions {Emmott:2019jp}. Within this network of interactions,
616 the NS1/2 protein interacts with the viral RNA polymerase NS7, which in turn binds
617 VPg. It is therefore possible that the interactions observed between the NS1/2
618 proteins and the host proteins involved in translation, occurs via the formation of a
619 NS1/2-NS7-VPg complex. How the viral protein-protein interactions within the
620 replication complex integrate with the network of cellular proteins identified in the
621 current study and how this facilitates viral replication and/or regulates the host
622 response to infection, remains to be determined.

623 This study provides an unprecedented insight into the identity of host factors likely
624 involved in the norovirus life cycle. As detailed above, we focused our detailed
625 analysis on the role of G3BP1 given that it was identified in all three screens,
626 however it is likely that many of the host factors identified in each screen play key
627 roles in the norovirus life cycle. The high enrichment of proteins involved in vesicle-
628 mediated transport, organelle organization and exocytosis, fits well with our current
629 understanding on the nature of the norovirus replication complex and the impact on
630 host cell processes. Detailed analysis of the impact of norovirus non-structural

protein expression and MNV infection on host cell membrane architecture suggests that norovirus replication complexes are generated from the endoplasmic reticulum (ER), and results in the formation of single membrane vesicles (SMVs), double membrane vesicles (DMVs) and multi membrane vesicles (MMVs) {Doerflinger:2017fp}. The process by which the non-structural proteins induce the formation of these structures is unknown, but the NS1/2 and NS4 proteins are thought to be key to the process. We have previously reported that the NS1/2 protein from MNV and HuNoV interacts with the VapA and VapB proteins and that this interaction is required for efficient viral replication {McCune:2017ev}. The norovirus NS4 protein associates with lipid droplets and is able to drive the formation of SMVs and DMVs {Doerflinger:2017fp}, suggesting that it may regulate the biosynthetic pathways involved in lipid synthesis or intracellular vesicular transport pathways. Our characterisation of the replication complex indicates an intimate link with numerous proteins involved in vesicle transport and lipid metabolism (Figure 2-figure supplement 1). Given that NS1/2 and NS4 interact to form a complex {Emmott:2019jp}, it is likely they work in concert to drive the formation of membrane-bound replication complex by regulating the functions of multiple components, the characterisation of which will require further analysis.

In conclusion, our data adds significantly to the growing body of literature on the role of G3BP proteins in the life cycle of viruses and further extends the functional roles of G3BP1 to include the promotion of viral translation processes. We identify G3BP1 as a host protein that has a critical role in the life cycle of murine and human noroviruses, identifying the first cellular pro-viral protein with pan-norovirus activity. Furthermore, given the apparent importance of G3BP1 to an early stage of the

norovirus life cycle, this work suggests that targeting G3BP1 may hold future therapeutic potential.

Grants:

CBW was supported by NIH K08 AI128043 and Burroughs Wellcome Fund. MAM was supported by NIH U19 AI109725. IG is a Wellcome Senior Fellow. This work was supported by funding from the Wellcome Trust (Refs: 207498/Z/17/Z and 104914/Z/14/Z) and the Biotechnology and Biological Sciences Research Council UK (Refs: BB/N001176/1and BB/000943N/1). JBE was supported by a Churchill Scholarship.

Acknowledgments:

The authors would like to thank Skip Virgin (Washington University in St. Louis) for intellectual input and the provision of reagents and resources. Kate Heesom of the University of Bristol Proteomics facility for support with the mass spectrometry analysis and Nerea Irigoyen (University of Cambridge) for help with polysome profiling.

Figure Legends

Figure 1. **The norovirus VPg proteins interacts with ribosome associated translation initiation factors.** A) Amino acid sequence alignment of the GV murine norovirus VPg sequences with VPg from representative human noroviruses from GI Norwalk virus (NV), GII, and GIV. The position of the site of RNA linkage to the highly conserved tyrosine residue is highlighted in green. The eIF4G binding motif is boxed and the position of the C-terminal single amino acid change known to interfere with eIF4G binding highlighted in orange. B) m7-GTP sepharose was used to affinity purify eIF4F containing complexes from either wild-type BHK cells (BHK) or BHK cells containing the Norwalk virus (NV) replicon (BHK-NV). Samples of the lysate (L) or the affinity purified complexes (m7) were separated by SDS-PAGE then analysed by western blot for the indicate proteins. Molecular mass shown on the left of the gels represent the positions of molecular weight markers. C) GFP fusion proteins to either the wild type (WT) or C-terminal eIF4G binding domain mutants of the MNV and NV VPg proteins (F123A, F137A) were transfected into human 293T cells and subjected to immunoaffinity purification using anti-GFP. Samples of the input lysates (Input) and the purified complexes (GFP-IP) were then separated by SDS-PAGE and analysed by western blot analysis for the indicated proteins. Mock transfected cells served as a specificity control. The approximate expected molecular mass of each protein is shown to the left. D) Quantitative proteomics was used as described in the text to identify host factors that were affinity purified following transfection of GFP-tagged derivative of either the NV or MNV VPg proteins. Proteins specifically enriched in comparison to the GFP control are shown. Data visualisation was performed using Cystoscape (Shannon et al., 2003) . E) Western blot analysis of cell

extracts (Input) or immunoprecipitated (GFP IP) complexes isolated from cells transfected as described in panel C. For clarity, the molecular masses shown in this panel refer to the expected mass of the protein being examined.

Figure 1-Figure Supplement 1: Host factors binding to the norovirus VPg. Quantitative proteomics was used as described in the text to identify host factors that were affinity purified following transfection of GFP-tagged derivative of either the NV or MNV VPg proteins. Proteins specifically enriched on the murine norovirus or human norovirus (Norwalk) VPg proteins in comparison to the GFP control are shown in panels A and B respectively. Proteins that were identified as enriched in at least two of the three biological repeats were counted as potential binding proteins and the SILAC ratios were computed as the average of the two or three biological repeats. The raw values used to compute this figure are presented in Supplementary file 1. Panel C illustrates the proteins previously found to interact with the 5' or 3' termini of the MNV genome (Bailey et al., 2010; Vashist et al., 2012b) or to associate with MNV VPg using tandem affinity purification (Chung et al., 2014). Data visualisation was performed using Cystoscape (Shannon et al., 2003)

Supplementary File 1: Raw data associated with figure 1. A) Log2 SILAC ratio of proteins identified in Norwalk virus (NV) VPg GFP Trap pull downs. The experimental details are provided in the materials and methods. SILAC ratios were computed by comparing the ratio of the peptides for each protein in the GFP control pull down to that obtained with the NV-GFP fusion protein. As described in the text each experiment was performed in three independent conditions varying the label in each biological sample. M/L – medium vs light sample, H/L – heavy vs light labelled

730 sample and M/L – medium vs light sample. B) As described in panel A but as
731 obtained using the MNV VPg-GFP fusion protein as the bait.
732
733 **Figure 2: Proteomic characterisation of the norovirus replication complex**
734 **using infectious epitope tagged MNV.** A) Schematic representation of NS1/2-
735 FLAG and NS4-FLAG viruses contain insertions of nucleotide sequences encoding
736 the FLAG peptide DYKDDDDK (in yellow) in their coding sequences. The NS1/2-
737 FLAG virus FLAG peptide was inserted between 2 of the 3 caspase-3 cleavage sites
738 present in NS1/2 (underlined). B) BV2 cells labelled with stable derivatives of
739 arginine and lysine were infected with either wild type MNV (WT) or recombinant
740 epitope-tagged MNV as described in the materials and methods. 12 hours post
741 infection samples were lysed, samples pooled and immunoaffinity purifications
742 performed as described in the text. Samples of the cell lysates (Input) and the affinity
743 purified complexes (IP:Flag) were analysed by SDS-PAGE on a 4-12% gradient gel
744 prior to silver staining. The positions of the NS1/2, NS2 and NS4 proteins is shown.
745 C) Western blot analysis of lysates purified from cells infected as described in panel
746 B, for various viral proteins, confirming the specific enrichment of viral replicase
747 components. D) Plot comparing the proteins identified in the complexes purified from
748 cells infected with the NS1/2 and NS4 Flag expressing viruses. The raw data
749 associated with this figure is presented in Supplementary file 2. Proteins identified in
750 at least two of the three biological repeats are shown. SILAC ratios were calculated
751 as an average of the two or three biological samples. All MNV proteins were
752 identified in association with NS1/2 and NS4 (light blue) including the viral
753 polymerase NS7, demonstrating enrichment of the MNV replication complex.
754 Proteins previously identified as host factors potentially involved in some aspect of

the norovirus life cycle through various biochemical or genetic screens are shown in red. Selected highly enriched proteins are highlighted in black. The NS1/2 binding partner VapA (McCune et al., 2017) and paralog VapB were both enriched by NS1/2 and NS4.

Figure 2-Figure Supplement 1: Additional analyses of NS1/2 and NS4-associated proteins. MNV proteins highlighted in light blue, and G3BP1 in gold. A) Gene ontology using PANTHER overrepresentation analysis of proteins copurifying with NS1/2 or NS4 (Log2 SILAC ratio >2 for either protein). Proteins in selected, mutually exclusive gene ontology categories are plotted in different colors as depicted .B) A number of factors previously identified as MNV host factors using proteomics or CRISPR approaches {Orchard:2019je, Chung:2014dd, Vashist:2012ke} copurified in pulldowns of NS1/2 and NS4 (highlighted red). C) Novel putative MNV host factors highly enriched (Log_2 SILAC ratio >4 for either protein) by NS1/2 and NS4 are plotted in black. D) Proteins identified in pulldowns of NS1/2 and NS4 which were also identified in pulldowns of MNV VPg are plotted in red. E) Proteins enriched in pulldowns of NS1/2 and NS4 which were also identified using CRISPR screening as MNV host factors are plotted in red (positive host factors) and yellow (negative host factors), along with G3BP1 in gold.

Figure 2-Figure Supplement 2: Further analysis of proteins enriched through MNV VPg proteomics and FLAG-tagged virus replication complex proteome data (Log_2 SILAC ratio >1). A) Venn diagram illustrating the degree of overlap between the proteins identified in the three proteomics approaches. The greatest overlap between VPg and the replication complex proteome data was observed between VPg and

NS1/2. G3BP1 was enriched in pulldowns of all three bait proteins (VPg, NS1/2 and NS4). B) The baits NS1/2 and NS4 both enriched VPg during replication complex pulldowns, but NS1/2 also enriched the VPg binding partner eIF4G, while NS4 did not. Immunoblot analysis revealed that NS4 enriched primarily the NS4/5 (VPg) polyprotein precursor, and not mature VPg, while NS1/2 enriched primarily the mature form of VPg (Figure 2C). C) Plot of all MNV VPg binding partners identified in Figure 1 which overlapped with proteins associated with the replication complex through NS1/2 and NS4 purification. Most VPg interaction partners were better enriched by NS1/2 than NS4, except G3BP1. D) Table showing Gene Ontology analysis of proteins enriched by VPg and NS1/2 during infection using PANTHER overrepresentation analysis, revealing a subset of the replication complex dedicated to translation and RNA metabolism.

Supplementary File 2: Raw data associated with figure 2. A) Log2 SILAC ratio of proteins identified anti-FLAG immunoprecipitations from cells infected with the NS1/2 tagged MNV. The experimental details are provided in the materials and methods. SILAC ratios were computed by comparing the ratio of the peptides for each protein in the anti-Flag immunoprecipitations performed on cells infected with wild type MNV. As described in the text each experiment was performed in three independent conditions varying the label in each biological sample. M/L – medium vs light sample, H/L – heavy vs light labelled sample and M/L – medium vs light sample. The Log2 transformed values and the average values are shown. B) As described in panel A but as obtained using the NS4-FLAG tagged MNV. C) Combined dataset obtained using NS1/2 and NS4 tagged viruses showing the average Log2 SILAC ratios.

Supplementary file 3: Gene ontology and cross comparison analysis of the data obtained in Figure 2. A). Gene ontology of the host proteins found to be enriched by both NS1/2 and NS4. B) PANTHER overexpression analysis of host proteins found to be enriched by both NS1/2 and NS4. C) Raw data used for PANTHER analysis shown in panel B. D) Colour code for data shown in panel C. E) List of host proteins identified in previous studies as having (potential) roles in the norovirus life cycle along with their degree of overlap with the host proteins identified using NS1/2 and NS4. F) Gene ontology analysis of host proteins identified as binding to the MNV NS1/2 protein and enriched using GFP-tagged MNV VPg.

Figure 3: CRISPR screen identifies host genes positively and negatively selected upon MNV infection. A) Schematic overview of the infection CRISPR screen workflow. BV2 cells expressing Cas9 were transduced with a CRISPR library then subsequently infected with either MNV CR6 or CW3 for 24 hours. Cells remaining after 24 hours were harvested and used for guide RNA abundance analysis as described in the text. B) Volcano plot identifying candidate genes enriched upon MNV-CW3 (red) or MNV-CR6 (blue); red or blue labelled genes correspond to the top-ten positive or negatively selected genes ranked by the STARS algorithm. C) Plot comparing the Log2 fold change in guide RNA abundance in the CRISPR library transduced BV2 cells following infection with either CR6 or CW3 MNV.

Supplementary File 4. Raw data and further analysis of the data obtained in figure 3. A) List of genes ranked with a positive STARS obtained with the Brie CRISPR screen against MNV CW3. B) List of genes ranked with a negative STARS

obtained with the Brie CRISPR screen against MNV CW3. C) As in panel A except using the MNV strain CR6. D) As in panel B except using the MNV strain CR6. E) Combined STARS ranking for the genes in both MNV CW3 and CR6 data sets. F) Comparison of genes with positive and negative STARS values in the data sets obtained using MNV CW3 and CR6. G) Comparison of data from panel A and C with the previous MNV CRISPR screens. H) Gene ontology overexpression analysis of genes identified in this study as having positive STARS values for both MNV CW3 and CR6.

Supplementary File 5. Comparison of data obtained from three screens to identify host factors involved in the norovirus life cycle. A) Comparison of the data obtained using MNV VPg-GFP trap with the MNV NS1/2 and NS4-FLAG tagged purifications. B) Comparison of the data obtained using the CRISPR screen and the MNV NS1/2 and NS4-FLAG tagged purifications. C) Comparison of the data obtained from all three screens.

Figure 4: CRISPR knockout of G3BP1 renders cells non permissive for MNV replication. A) Western blot analysis of three independent ΔG3BP1 clones for GAPDH, G3BP1 and G3BP2. B) High multiplicity, single cycle growth curve analysis of the impact of G3BP1 ablation on MNV replication. BV2 ΔG3BP1 clone C cells were infected at a MOI of 10 TCID50/cell, samples were collected at the time points illustrated, the samples then processed and titrated by TCID50 as described in the text. The error bars represent standard errors of three biological repeats and the data are representative of at least three independent experiments. C) Wild type (WT) or ΔG3BP1 clone C BV2 cells were plated in a 96 well plate and subsequently

infected using a serial dilution of either EMCV or MNV. Cells were fixed in paraformaldehyde and stained with crystal violet 5 days post infection. D) Light micrographs of WT or ΔG3BP1 cells either mock infected (-) or infected with EMCV or MNV and visualised 5 days post infection.

Figure 5. G3BP1 is required for human Norwalk virus replication in cell culture. A) Colony formation ability of human norovirus VPg-linked RNA isolated from BHK-NV replicon containing cells is dependent on the presence of VPg. NV VPg-linked RNA isolated from BHK-NV cells was either mock treated or treated with proteinase K prior to transfection into BHK cells. Wells were transfected with either 1.5μg or 0.75μg of total RNA isolated from NV replicon containing BHK cells. Following 2 weeks of antibiotic selection with G418, surviving replicon containing colonies were fixed and stained with crystal violet in paraformaldehyde. B) NV replicon colony forming assay in WT and G3BP1-/- U2OS cells performed as described in panel A, with the exception that colonies were stained 12 days post transfection. C) Quantification of NV replication in WT or ΔG3BP1 U2OS cells following transfection of viral VPg-linked RNA. Viral RNA was quantified by RT-qPCR following transfection and antibiotic selection. The error bars represent the standard error of three biological repeats and are representative of three independent experiments. D. Analysis of the impact of loss of G3BP1 on NV replication in BV2 cells. Wild type BV2 cells, ΔG3BP1 BV2 cells or ΔG3BP1 BV2 cells reconstituted with wild type full length G3BP1 were transfected with NV replicon VPg-linked RNA. Following selection with G418 for 3 weeks, the cells were fixed and stained with toluidine blue to facilitate the visualization of microcolonies. Pictures of the entire well and three independent fields of view are shown.

Figure 6: MNV replication in BV2 cells requires the RNA binding activity of G3BP1. A) Schematic illustration of the G3BP1 truncations used to identify the domains involved in the norovirus life cycle. The positions of the various domains including the RRM and RGG domains deleted in the ΔRGG and ΔRGG/ΔRRM mutants are also shown. Western blot analysis of wild type BV2 cells (WT) or a ΔG3BP1 cells (clone 1B2) and the respective complemented lines expressing either WT or the various G3BP1 truncations. Cells were lysed prior to separation by 12% SDS-PAGE. B) WT or ΔG3BP1 cells complemented with the indicated constructs were plated in a 96 well plate then infected with a serial dilution of MNV, before being fixed and stained 5 days post infection as described in the text. C) WT or ΔG3BP1 cells complemented with the indicated constructs were infected with MNV at an MOI of 10 TCID50 per cell. After 24 hours the virus yield was determined by TCID50. The error bars represent the standard error of three independent repeats. The data are representative of at least two independently repeated experiments.

Figure 7: Loss of G3BP1 results in a defect following transfection of viral VPg-linked RNA into ΔG3BP1 cells. A) The indicated cell lines were transfected with MNV viral RNA and harvested at 9 hours post transfection for TCID50 to assess the virus yield. In some instances, the nucleoside analogue 2CMC was included to inhibit viral replication. The dotted line indicates the limit of detection (LOD) and the error bars represent the standard error from three biological repeats. B) Infectious virus yield from ΔG3BP1 and reconstituted cell lines performed as described in panel A. C) and D) illustrate the accompanying western blots for samples prepared in panel A and B respectively. Samples were prepared at 24 hours post transfection,

prior to harvesting, separation by SDS-PAGE on a 4-12% gradient gel prior to western blotting for the indicated proteins.

Figure 8: The Lack of G3BP1 results in a failure to produce viral negative sense RNA. The experimental design is illustrated in A. Wild type or ΔG3BP1 (1B2) cells were infected prior to the addition of the nucleoside analogue 2CMC to prevent viral RNA synthesis. Samples were harvest at the indicated time post infection and viral positive (B) and negative sense RNA quantified by stand specific RT-qPCR (C). Error bars represent standard error of three biological repeats. LOD refers to the limit of detection of the assay. D) and E) Viral RNA synthesis following transfection of viral VPg-linked RNA into WT or two ΔG3BP1 cell lines. F) and G) Viral RNA synthesis following transfection of viral VPg-linked RNA into ΔG3BP1 (1B2) complemented with full length G3BP1 or truncated derivatives. Error bars represent standard error of three biological repeats.

Figure 9: G3BP1 is required for the association of VPg and norovirus VPg-linked RNA with ribosomal subunits. A) GFP-Trap immunoprecipitation of complexes isolated on with GFP alone or GFP tagged wild type MNV-VPg demonstrating the pull down of eIF4G1, G3BP1 and 40S subunits (RpS6). BV2 cells were transfected with the relevant constructs, lysates prepared and GFP-Trap pull downs performed as detailed in the text. Samples were separated by SDS-PAGE and western blotted for the proteins as shown. B) Mutations in the eIF4G binding domain ablate the association of VPg with G3BP1 and ribosomal subunits and the reconstitution of G3BP1 expression in ΔG3BP1 BV2 cells restores the interaction. GFP-Trap pull downs were performed as described in panel A with the addition of

930 the MNV VPg F123A mutation known to reduce the association with eIF4G and the
931 inclusion of the in ΔG3BP1 1B2 cell line engineered to express a Flag-tagged
932 derivative of G3BP1. Following the pull down samples were analysed by western blot
933 for presence of the ribosomal subunits using RpS6 and RpL4 as markers for the
934 small and large ribosomal subunits respectively. > denoted the RpL4 proteins
935 whereas * indicated the presence of GFP-VPg fusion proteins, present on the same
936 membrane due to the sequential probing of the membrane. C) Loss of G3BP1
937 results in decreased association between norovirus RNA and ribosomal proteins. WT
938 or cells lacking G3BP1 were infected with MNV in the presence of the RNA
939 polymerase inhibitor 2CMC and the amount of viral RNA found associated with RpS3
940 determined by RNA-IP. Error bars represent SEM of duplicate samples and the
941 values are expressed as fold enrichment with respect to the IgG control antibody.
942
943 **Figure 9-Figure Supplement 1. G3BP1 is required for the association of VPg**
944 **with ribosomal subunits.** GFP-Trap pull down was performed as described in
945 figure 9 following transfection of GFP tagged derivatives of either a WT or a F123
946 MNV VPg proteins into WT BV2 cells, ΔG3BP1 BV2 cells or ΔG3BP1 BV2 cells
947 engineered to express Flag tagged derivative of WT G3BP1. Following the GFP-
948 Trap pull down, samples of the input and purified complexes were analysed by
949 western blot for the proteins as shown.
950
951 **Figure 10: G3BP1 is required for polysome association of viral RNA**
952 **association.** A) Polysome profiles of the ribosome containing fractions from mock or
953 MNV infected wild type (WT) or ΔG3BP1 (1B2) BV2 cells at 4 and 9 hours post
954 infection (moi 3 TCID50/cell). B) Relative viral RNA levels present in ribosome

containing fractions expressed relative to WT infected BV2 cells. C) Extended gradient fractionation of WT or ΔG3BP1 cells infected with MNV and harvested 9 hours post infection. Viral RNA levels across the gradient are expressed as described in panel B. Error bars represent standard error of three technical repeats from each biological samples, defined as a single fraction from a single experiment. The data shown in panels A-C are representative of at least three experimental repeats.

Figure 11: G3BP1 is required for efficient norovirus VPg-dependent translation.

A) Illustration of the bicistronic construct used to assess the *in* vitro translation efficiency of the extracts prepared from WT BV2 cells or cells lacking G3BP1. The location of the 5' cap and the 3' poly (A) tails are highlighted in relation to the renilla and firefly luciferase coding regions, along with with the CrPV IRES. Comparsion os cap (B) and CrPV-IRES dependent translation (C) in translation competent extracts prepared from WT BV2 cells or BV2 cells lacking ΔG3BP1. Extracts were programmed with *in vitro* transcribed RNA as described in the text and the levels of luciferase compared to those obtained using rabbit reticulocyte lysate (RRL). D) Translation of MNV VPg-linked viral RNA is diminished in nuclease treated extracts prepared from ΔG3BP1 cells. Translation of viral RNA in rabbit reticulocyte lysates (RRL) was used as a side by side comparison. The positions of the viral proteins quantified by phosphor imaging are indicated with arrow heads (1-5). E) Quantification of norovirus protein synthesis for each of the identified protein products in panel D and total translation levels across multiple experiments. The levels of viral translation is expressed as a percentage relative to the same protein

product translated in extracts prepared from WT cells. The error bars represent the standard error of three independent experiments. F) Norovirus VPg-dependent translation in non-nuclease treated extracts prepared from WT or ΔG3BP1 cells. The total translation efficiency for the viral proteins, highlighted by arrowheads, is shown below the respective lane. Translation efficiency is expressed as a percentage in comparison to the average of translation seen in extracts prepared from WT cells across all biological repeats. E) Quantification of viral proteins produced in panel (D) plotted as % translation efficiency with respect to the translation levels observed in non-nuclease treated extracts from WT BV2 cells..

Figure 11-Figure Supplement 1: A) Characterisation of viral VPg-linked RNA. The sensitivity of purified MNV VPg-linked RNA to various nucleases was compared to *in vitro* transcribed capped MNV gRNA (cap-gRNA) and the MNV1 full length cDNA construct. RppH was included as a decapping enzyme require for Xrn1-mediated cleavage of capped RNAs. Following digestion, the samples were analysed on a 1% native agarose gel. B) In vitro translation of viral VPg linked RNA in rabbit reticulocyte lysates demonstrated robust translation and the production of a protein profile indistinguishable from in vitro transcribed capped genomic RNA (cap-g). Capped sub-genomic (cap-sg) RNA was included to demonstrate the location of the VP1 and VP2 proteins. C) The translation of MNV VPg-linked RNA in extracts prepared from ΔG3BP1 cells is reduced across multiple time points. *In vitro* translations prepared in rabbit reticulocyte lysates (RRL) using *in vitro* transcribed capped genomic RNA (cap-g) or capped sub-genomic (cap-sg), along with viral VPg-linked RNA, was used as a reference for the expected mass of the viral proteins.

Materials and methods.

Cells. The murine microglial BV2 cell line (Blasi et al., 1990) was provided by Jennifer Pocock (University College London). BV2 cells were maintained in DMEM supplemented with 10% FCS (Biosera), 2 mM L-glutamine, 0.075 % sodium bicarbonate (Gibco) and the antibiotics penicillin and streptomycin. BHK cells engineered to express T7 RNA polymerase (BSR-T7 cells, obtained from Karl-Klaus Conzelmann, Ludwid Maximillians University, Munich, Germany) were maintained in DMEM containing 10 % FCS, penicillin (100 SI units/ml) and streptomycin (100 µg/ml), and 0.5 mg/ml G418. U2OS cells and derivatives of them were obtained from Nancy Kedersha (Harvard Medical School). All cell lines were screened for mycoplasma and confirmed as negative. The identity of the cell lines was not confirmed by STR profiling.

Generation of G3BP1 KO cells. BV2 cells were cultured in DMEM containing 10% FBS and 1% HEPES. G3BP1 knockout BV2 cells were generated using two approaches. The clone 1B2 was generated by transiently transfected with Cas9 and a sgRNA (5TTCCCCGGCCCCGGCTGATGNGG) targeting exon 7 of G3BP1. BV2 cells were then single cell cloned and G3BP1 was sequenced by Illumina HiSeq. BV2 cells are polyploid at the G3BP1 locus as described previously (Orchard et al., 2016). Clone 1B2 also had three independent deletions at the sgRNA binding site resulting in deletions of 1, 2, and 5 base pairs respectively. The mutations introduced into the IB2 BV2 cell clone resulted in frame shifts at nucleotide positions 253, 254 and 244 and the absence of detectable G3BP1 protein as measured by western blot. G3BP1 knockout BV2 cell clones A, C and F were generated using an independent approach that relied on first generating a pool of three lentiviruses carrying guide

RNAs TGTGCAACATGTCCGGGGCC, CAAACTCCCGCCCGACCAGC and TAGTCCCCTGCTGGTCGGGC targeting the first 100bp of the coding sequence, cloned into pLentiCRISPRv2 (Sanjana et al., 2014). BV2 cells were then transduced with the pool of 3 lentiviruses, selected by puromycin treatment for 72 hours, prior to cloning by limiting dilution. Individual clones were then screened by western blot for the absence of G3BP1.

G3BP1 complementation. Mouse G3BP1 cDNAs were subcloned into pCDH-MCS-T2A-puro-MSCV lentiviral vector (System Biosciences) by NEBuilder HiFi DNA assembly (New England Biolabs). Mouse G3BP1 was subcloned from pCM6-G3BP1 (MR207441; Origene). Mouse G3BP1 lentiviral constructs deficient in the C-terminal RGG domain (mG3BP1ΔRGG) and the RGG and RRM domains (mG3BP1ΔRGGRRM) were generated by Gibson cloning from the pCMV6-G3BP1 vector. Lentivirus was generated by co-transfecting pCDH-G3BP1-T2A-puro-MSCV with pCMV-VSV-G and pSPAX2 into 293T cells with Trans-IT LT1 (Mirus Biosciences) per manufacture instructions. Two days post-transfection, supernatants were harvested, filtered through a 0.22 micron filter, and stored at -80C. Lentivirus encoding G3BP1 or an empty control was then used to transduce G3BP1 KO 1B2 BV2 cells. Two days post-transduction BV2 cells were selected with puromycin (2.5ug/ml) for six days.

MNV growth curves

To determine the effects of G3BP1 disruption on MNV replication G3BP1 WT, KO, or complemented cells were plated in each well of a flat bottom 96-well plate and then infected with either MNV strains CW1, CW3, or CR6 as described in the text.

Infected cells were flash frozen at -80°C at the times post infection indicated in the text. Viral replication was then assessed by plaque assay or TCID50 in BV2 cells as described in the text. In cases where the appearance of virus-induced cytopathic effect was examined, infected monolayers were either visualized by light microscopy directly or fixed with crystal violet in formalin, prior to washing and imaging.

CRISPR screens. The CRISPR screen was performed similarly to that described previously (Orchard et al., 2016) with a number of modifications that included the use of the Brie gRNA library to reduce off target effects (Doench et al., 2016) and shorter infection times to improve the recovery of gRNAs that may also compromise cell viability. BV2 cells stably expressing Cas9 nuclease (Orchard et al., 2016) were transduced with the Brie library using previously described protocols (Doench et al., 2016). MNV strains CW3 and CR6 were used to infect BV2 CRISPR library at MOI 5 pfu/cell and cells were isolated 24 hours post infection and preparation of gDNA for sequencing as described previously (Orchard et al., 2016). The screen relies on the premise that guide RNAs targeting genes that are overrepresented following infection represent genes that when disrupted are protected against infection and therefore likely represent factors with pro-viral activity. Likewise, genes for which guide RNA are underrepresented suggest that infection had proceeded faster and the gene is anti-viral. Following sequencing, the data was analyzed by STARS method as previously described (Doench et al., 2016; Orchard et al., 2016). Visualization of candidate genes was accomplished using R (RStudio, Inc., Boston, MA).

Maintenance of SILAC cell lines. Stable isotope labelling of amino acids in cell culture of BV2 cells (SILAC, Ong et al., 2002), was carried out in high-glucose DMEM lacking arginine and lysine (Sigma-Aldrich), supplemented with dialyzed fetal bovine serum, 1% L-glutamine, 1X nonessential amino acids, 10 mM HEPES, and 1X penicillin/streptomycin. SILAC media were supplemented with Light (R0K0), Medium (R6K4) or Heavy (R10K8) Arginine and Lysine (Cambridge Isotope Laboratories). BV2 cells were maintained in SILAC medium for 2 weeks to ensure complete metabolic labelling of proteins. Labelling of HEK-293T cells was performed essentially as described for BV2 cells, with the omission of 10 mM HEPES and 1X non-essential amino acids from the cell culture media.

DNA based recovery of murine norovirus. Experiments were performed according to previously published protocols (Chaudhry et al., 2007). Briefly, BSRT7 cells were infected to an MOI of 0.5-1 PFU/cell with fowlpox virus expressing T7 RNA polymerase. Cells were then transfected with a plasmid encoding the MNV full length clone, or a derivative thereof (e.g. pT7 MNV 383FLAG 3'Rz or pT7 MNV 2600FLAG 3'Rz, our FLAG-tagged virus constructs containing FLAG tags in either NS1/2 or NS4 respectively). MNV was harvested by freeze-thaw at 24h post-transfection.

To generate higher titre stocks, WT MNV, NS1/2-FLAG MNV, and NS4-FLAG MNV (Thorne et al., 2012) generated using the DNA based recovery method described above were passaged once in BV2 cells. After 80-90% of cells displayed visible cytopathic effects (CPE) of viral infection, flasks containing infected cells were frozen at -80^{o}C. Flasks were frozen and thawed twice before cell debris was removed by centrifugation at 4000 rpm for 10 minutes in a benchtop centrifuge. Viruses were

pelleted by centrifuging over a 30% sucrose cushion at 76,755xg in a SW32ti rotor for 2 hours at 4^{o}C. Virus pellets were resuspended overnight in PBS to achieve 100-fold concentration. Concentrated virus was then passed through a 23-gauge blunt needle 15 times, and clarified by centrifugation at maximum speed in a benchtop microcentrifuge for 10 minutes. Supernatant aliquoted, and titrated prior to use.

Infection of SILAC labelled BV2 cells with FLAG-tagged viruses. SILAC-labelled BV2 cells were infected with WT MNV, NS1/2-FLAG or NS4-FLAG viruses at an MOI of 10 TCID50 cell. Infections were performed in triplicate, using different combinations of SILAC-labeled BV2 cells each time to control for any impact of the SILAC labelling. Infected cells were then plated in the appropriate SILAC media. At 10 hours post-infection, cells were harvested by scraping, and pelleted at 500xg for 5 minutes. Cells were then washed 3 times with ice-cold PBS, and were lysed in (0.5% Nonidet-P40 substitute, 10 mM Tris-HCl pH 7.5, 150 mM NaCl, 0.5 mM EDTA, 2 mM MgCl). Benzonase nuclease (Sigma-Aldrich) was added to lysis buffer to a concentration of 5 μl/ml to prevent nonspecific interactions mediated by RNA or DNA.

Transfection of SILAC labelled HEK-293T cells with GFP-tagged VPg. SILAC-labelled HEK-293T cells were transfected with pEGFP-C1 (control) or derivatives thereof containing either human or murine norovirus VPg protein as described in Emmott & Goodfellow, (2014). GFP fusions of both wild-type protein or mutant VPg containing a mutation to inhibit initiation factor binding (MNV: F123A, HuNoV: F137A) were used. Cells were transfected using Lipofectamine 2000 (Life Technologies) according to the manufacturers protocol, using antibiotic-free SILAC

media in place of Opti-mem. The experiment was performed in triplicate and SILAC labels switched in one of the replicates.

FLAG and GFP-TRAP immunoprecipitation. FLAG immunoprecipitations were performed following the manufacturer's protocol (FLAG M2 beads, Sigma Aldrich) as described (Thorne et al., 2012). In brief, protein concentration in lysates was normalized using BCA. Lysates were then diluted with 1 volume of wash buffer (10 mM Tris-Cl pH 7.5, 150 mM NaCl, 0.5 mM EDTA). Equal volumes of anti-FLAG affinity gel were dispensed into either WT infected cell lysates, or lysates of cells infected with NS1/2-FLAG or NS4-FLAG. Binding was carried out overnight at 4^{o}C with rotation. After binding, beads were washed 3 times with wash buffer. All liquid was carefully removed from each tube, before boiling in SDS-PAGE loading buffer for 10 minutes. GFP-trap immunoprecipitation of GFP-tagged VPg was accomplished using GFP-trap beads (Chromotek) per the manufacturer's protocol, as described (Emmott and Goodfellow, 2014). RNase cocktail (Ambion) was also included in the lysis buffer at a concentration of 5 μl/ml to prevent non-specific interactions mediated by RNA. In all cases, light, medium, and heavy-labelled proteins eluted from the beads for each experimental replicate were pooled together in a ratio of 1:1:1 before submission for mass spectrometry analysis at the University of Bristol Proteomics Facility.

Mass spectrometry analysis. Mass spectrometry analysis was performed at the University of Bristol Proteomics Facility. In brief, samples were run into precast SDS-PAGE gels for 5 minutes, the entire sample cut from the gel as a single band, and then subjected to in-gel tryptic digestion including reduction and alkylation using a

ProGest automated digestion unit. The resulting peptides were fractionated using a Dionex Ultimate 3000 nanoHPLC system in line with an LTQ-Orbitrap Velos or Orbitrap Tribrid Fusion mass spectrometer.

Interpretation of SILAC Proteomics data. Raw data files were processed and quantified using Maxquant v1.5.5.1 or 1.6.0.16 (Tyanova *et. al.* 2016). The GFP-VPg experiments were searched against the Uniprot human database (70,550 entries, downloaded September 19th 2016) plus a custom FASTA file containing the wild-type and mutant VPg sequences. The raw data, search results and FASTA files can be found as part of PRIDE submission PXD007585 (Reviewer username: reviewer75984@ebi.ac.uk, Password: BH2pTctW). The FLAG-virus experiments were searched against the Uniprot mouse database (Swiss-prot only, 16,966 entries, downloaded May 19th 2018) plus a custom FASTA file containing the various Murine norovirus proteins. The raw data, search results and FASTA files can be found as part of PRIDE submission PXD011779 (Reviewer username: reviewer49419@ebi.ac.uk, Password: eLYwivNP). Data were searched with default Maxquant parameters including upto 2 missed tryptic cleavages, oxidation of methionine and N-terminal acetylation as variable modifications, and carbamidomethylation of cysteine as a fixed modification. The data were searched against a reverse database and PSM and Protein FDR were set to 0.01. The requantify option was not selected.

GFP-VPg data were analysed as described previously (Emmott and Goodfellow, 2014). FLAG-virus experiments were analysed by computing the pairwise ratios of samples infected with NS1/2-FLAG or NS4-FLAG relative to WT MNV-infected

controls. Log_2 SILAC ratios for proteins identified in at least 2/3 replicates were averaged, and ratios for NS1/2-FLAG:WT and NS4-FLAG:WT were plotted for comparison of host cell proteins by viral replication complex-associated proteins.

Assessment of virus-induced cytopathic effect. BV2 WT, KO G3BP1 or respective G3BP1 complemented cells as described in the text, were seeded onto 96 well plates and infected with serial 10-fold dilutions (starting at MOI=10 TCID50/cell) of MNV (CW1) or EMCV. At 48h post-infection, cells were fixed in ice-cold methanol and stained with toluidine blue prior to washing and imaging.

Cap-Sepharose purification for eIF4F complex. Cell lysates were prepared from BHK parental cells or BHK containing GI Norwalk virus (BHK-NV) replicon cells in cap-Sepharose lysis buffer (100 mM KCl, 0.1 mM EDTA, 10% glycerol, 2 mM $MgCl_2$, 20 mM HEPES, pH 7.6 in KOH) with 1% TX-100, proteinase and phosphatase inhibitor cocktails (Calbiochem). Cytoplasmic extracts were centrifuged and RNase treated for 15 min at room temperature. At least 1000 µg of the cell lysates were incubated with Sepharose beads coupled to 7-methylguanosine (m^7GTP, Jena Biosciences). Input cell lysates were collected for western blot analysis while the remaining were incubated overnight with continuous rotation at 4°C. The eIF4F-enriched complex was precipitated and washed 2 times with cap-sepharose lysis buffer. Bound proteins were eluted in 2x reducing SDS-PAGE samples buffer and resolved by SDS-PAGE prior to western blot.

Human Norwalk virus colony formation assay. Total RNAs extracts from BHK or BHK-NV replicon-containing cells (Kitano et al., 2018) were pretreated with and

without proteinase K (10 µg/ml) in 10 mM Tris, pH 8.0, 1.0 mM EDTA, 0.1 M NaCl, and 0.5% SDS. Pretreated RNAs were immediately purified using GenElute RNA purification columns (Sigma). Serial 10-fold dilutions of mock or proteinase K-treated RNAs were transfected in BHK cells and 24 h post transfection, cells were passaged and maintained in growth media containing 0.5 mg/ml G418. Colonies began to form after 5 d and were allowed to grow until 14 d. All plates were harvested at day 14 and well-formed colonies were fixed in 10% formaldehyde and stained with toluidine blue. A similar protocol was followed to assess colony formation in U2OS cells with the exception that selections were maintained for up to 12 days post transfection. Where indicated, cell aliquots from each time point were collected for qRT-PCR analysis to assess viral RNA synthesis over time.

RNA co-immunoprecipitation. Coimmunoprecipitation of viral RNA with RpS3 and IgG, as irrelevant control, was performed using BV2 WT and BV2ΔG3BP1 clone lB2 cells inoculated with MNV1 at MOI of 50 TCID50 per cell in the presence of 400µM 2-CMC. Cell lysates equilibrated in EE buffer (50 mM HEPES, pH 7.0, 150 mM NaCl, 0.5% NP-40, 10% glycerol, 2.5 mM EGTA, 5 mM EDTA, 1 mM DTT, 100 ug/mL Heparin, and HALT protease and phosphatase inhibitor cocktail) as previously described were pre-incubated with antibody against either RpS3 or IgG for 12 h at 4°C with continuous rotation. Protein A/G Ultralink resin slurry (Thermo Fisher Scientific) was then added into cell lysates and antibody mixture and incubated further for 12 h at 4°C. Resin were washed with EE buffer 3x and the complex bound to the resin were eluted in 0.1M glycine, pH 2. Elutions were subjected to RNA extraction and bound viral RNA were quantitated by RT-qPCR.

Polyribosome fractionation analysis. BV2 WT and BV2 ΔG3BP1 cells were seeded at a density of 7.5 x 10^6 cells per T-75 flask, and then either mock infected or infected with MNV1 (CW1) at MOI 3 TCID50 per cell in the presence of 2-CMC (400μM) for each set of infection. After 1h, the inoculum was then removed; the cells were washed and maintained in growth media containing 2-CMC accordingly until the cells were harvested at 4h and 9h p.i. Prior to harvesting, cells were treated with cycloheximide (CHX) for 10 mins at 37°C (Sigma-Aldrich; 100 μg/ml) and were rinsed with 5 ml of ice-cold PBS supplemented with CHX 100 μg/ml. Polysome lysis buffer [20 mM Tris-HCl pH 7.5, 150 mM NaCl, 5mM MgCl, 1 mM DTT, 1% Triton X-100, 100 μg/ml cycloheximide, 25 U/ml TURBO DNase (Life Technologies)] was used to lyse the cells. Lysates were clarified by centrifugation for 20 min at 13,000 *g* at 4°C. Aliquots of the lysates were collected for BSA assay and qPCR analysis against MNV1 RNA before proceeding with fractionation. Input lysates were normalized to total protein concentration and RT-qPCR was used to confirm the levels of viral RNA in samples were comparable. Lysates were subjected next to 10-50% sucrose gradient centrifugation for 90 mins SW41Ti rotor at 190,000 *x g* at 4°C. The gradients were fractionated at 0.5 ml/min and the levels of RNA in each sample measured using an in line-254 nm spectrophotometer connected to a chart recorder. RNAs were extracted from each fraction, converted to cDNA and immediately used for qPCR. The distribution of viral RNA across the gradient was then calculated as percentage (%) of the viral RNA seen in WT BV2 cells using the reference gene (GAPDH) to obtain normalized values across the gradient. Samples were performed in duplicates on the same qPCR plate, and the observations were robust across three independent experiments. Data were collected using a ViiA 7 Real-Time PCR System (Applied Biosystems).

Transfection of VPg-linked MNV RNA into BV2 cells. VPg-linked RNA purified from MNV-1 virus particles was transfected in BV2 cells using NEON™ as previously described (Yunus et al., 2010). Total cell lysates were harvested at 3 and 9 hours post transfection with RIPA buffer. 10µg total lysates were analysed by 4-12% SDS-PAGE (Invitrogen) and antibodies against MNV, VPg, G3BP1 and GAPDH were used for detection using LI-COR® Odyssey® CLx. Virus yield was determined by $TCID_{50}$. For strand-specific qPCR detection of MNV RNA, total cellular RNA was extracted using GeneElute Mammalian Total RNA Miniprep kit (Sigma). RT-qPCR was performed as described previously (Vashist et al., 2012a).

Purification of MNV VPg-linked RNA. BV2 cells were infected at an MOI=0.01 $TCID_{50}$ per cell and harvested after ~30 post infection. Cell debris was removed by low speed centrifugation for 10 minutes and supernatant loaded onto 5 ml of 30% sucrose solution in PBS. MNV particles were pelleted using a SW32Ti rotor at 25,000 RPM for 4 hours at 4 ℃. Virus was then resuspended in PBS and total RNA extracted from soluble fraction. Where detailed, the authenticity of the viral RNA was examined by nuclease digestion. 500 ng of viral RNA or plasmid DNA was treated with DNase I (10U, Roche), XrnI+RppH (1U XrnI + 5U RppH, both from NEB) or RNase cocktail (0.5U RNase A + 20U RNase T1, ThermoFisher) at 37 ℃ for 10 minutes. Then analysed on 1% agarose gel.

Preparation of BV2 S10 cytoplasmic extracts. Preparation of BV2 S10 extracts was based on a previously published protocol (Rakotondrafara and Hentze, 2011; 2006). BV2 cells were harvested, washed with PBS, and lysed with 1x packed

volume of hypotonic buffer containing 10 mM HEPES pH7.6, 10 mM potassium acetate, 0.5 mM magnesium acetate, 5 mM DTT, 1x protease inhibitors cocktail (EDTA-free, Roche). Cells were lysed on ice for 45 minutes, then passed through 25G and 27G needles to achieve >95% lysis. Cell lysates were then centrifuged at 10,000 x g for 10 minutes at 4 ℃ twice and the supernatant collected. The total protein concentration was measured by Bradford assay and normalised to 20 mg/ml before freezing at -80 ℃ until use. For micrococcal nuclease treatment, S10 extracts were thawed on ice, 1 mM calcium chloride and 200 unit/ml final concentrations of micrococcal nuclease (NEB). Cell lysates were incubated at 25 ℃ for 15 minutes before adding 3 mM final concentration of EGTA was added.

***In vitro* translation of BV2 S10 lysates.** *In vitro* translation assays were set up based on a previous protocol (Favre and Trepo, 2001). Translation reactions were set up in 12.5 µl total volume containing 5 µl BV2 S10 lysate, 2.5 µl 5X translation buffer, 0.25 µl of 5 mg/ml creatine kinase, 1.25 µl RRL, 0.225 µl of 5 M potassium acetate, 0.25 mM of 100 mM magnesium acetate, 5.13 µCi ^{35}S-labelled methionine (PerkinElmer) and 10-100 ng/µl RNA as detailed in the text. 5X translation buffer contains 350 mM HEPES, 75 mM creatine phosphate, 10 mM ATP, 3.75 mM GTP, 100 µM amino acid minus methionine, 3.75 mM spermidine and 0.375 mM S-adenosyl-methionine. For control experiments using RRL (Promega), the reactions were set up according to manufacturer's instructions using 0.5-1 ng/µl RNA. Reactions were incubated at 30 ℃ for 90 minutes before addition of 12.5 µl trans-stop buffer containing 10 mM EDTA and 0.1 mg/ml RNase A and incubated at room temperature for 10 minutes, then 25 µl 5X loading buffer was added to the reaction and heated at 95 ℃ for 5 minutes. 10 µl lysates were resolved in 15% SDS-PAGE

and exposed to a phosphorimager screen and visualised using a TyphoonFLA7000 machine. For non-radioactive translation, 1.25 µl of 1 mM methionine was used instead of ^{35}S-labelled methionine, and the reactions were stopped with 100 µl 1x passive lysis buffer (Promega) and the luminescence read using a GloMax luminometer (Promega).

References:

Alam, U., and Kennedy, D. (2019). Rasputin a decade on and more promiscuous than ever? A review of G3BPs. Biochim Biophys Acta Mol Cell Res *1866*, 360–370.

Altan-Bonnet, N. (2017). Lipid Tales of Viral Replication and Transmission. Trends Cell Biol. *27*, 201–213.

Bailey, D., Carrara, G., Benson, A., Chaudhry, Y., Heeney, J., Yarovinsky, F., Simmonds, P., Goodfellow, I., McFadden, N., Shortland, A., et al. (2011). Norovirus regulation of the innate immune response and apoptosis occurs via the product of the alternative open reading frame 4. PLoS Pathog. *7*, e1002413.

Bailey, D., Karakasiliotis, I., Vashist, S., Chung, L.M.W., Rees, J., Reese, J., McFadden, N., Benson, A., Yarovinsky, F., Simmonds, P., et al. (2010). Functional analysis of RNA structures present at the 3' extremity of the murine norovirus genome: the variable polypyrimidine tract plays a role in viral virulence. J Virol *84*, 2859–2870.

Bartsch, S.M., Lopman, B.A., Ozawa, S., Hall, A.J., and Lee, B.Y. (2016). Global Economic Burden of Norovirus Gastroenteritis. PLoS ONE *11*, e0151219.

Blasi, E., Barluzzi, R., Bocchini, V., Mazzolla, R., and Bistoni, F. (1990). Immortalization of murine microglial cells by a v-raf/v-myc carrying retrovirus. J. Neuroimmunol. *27*, 229–237.

Brocard, M., Iadevaia, V., Klein, P., Hall, B., Lewis, G., Lu, J., Burke, J., Parker, R., Ruggieri, A., Goodfellow, I., et al. (2018). Norovirus infection results in assembly of virus-specific G3BP1 granules and evasion of eIF2α signaling. bioRxiv 490318.

Chang, K.-O., Sosnovtsev, S.V., Belliot, G., King, A.D., and Green, K.Y. (2006). Stable expression of a Norwalk virus RNA replicon in a human hepatoma cell line. Virology *353*, 463–473.

Chaudhry, Y., Nayak, A., Bordeleau, M.-E., Tanaka, J., Pelletier, J., Belsham, G.J., Roberts, L.O., and Goodfellow, I.G. (2006). Caliciviruses differ in their functional requirements for eIF4F components. J. Biol. Chem. *281*, 25315–25325.

Chaudhry, Y., Skinner, M.A., and Goodfellow, I.G. (2007). Recovery of genetically defined murine norovirus in tissue culture by using a fowlpox virus expressing T7 RNA polymerase. J. Gen. Virol. *88*, 2091–2100.

Chung, L., Bailey, D., Leen, E.N., Emmott, E.P., Chaudhry, Y., Roberts, L.O., Curry, S., Locker, N., and Goodfellow, I.G. (2014). Norovirus translation requires an interaction between the C Terminus of the genome-linked viral protein VPg and eukaryotic translation initiation factor 4G. J. Biol. Chem. *289*, 21738–21750.

Cotton, B.T., Hyde, J.L., Sarvestani, S.T., Sosnovtsev, S.V., Green, K.Y., White, P.A., and Mackenzie, J.M. (2017). The Norovirus NS3 Protein Is a Dynamic Lipid- and Microtubule-Associated Protein Involved in Viral RNA Replication. J Virol *91*, e02138–16.

Cristea, I.M., Rozjabek, H., Molloy, K.R., Karki, S., White, L.L., Rice, C.M., Rout, M.P., Chait, B.T., and MacDonald, M.R. (2010). Host factors associated with the Sindbis virus RNA-dependent RNA polymerase: role for G3BP1 and G3BP2 in virus replication. J Virol *84*, 6720–6732.

Doench, J.G., Fusi, N., Sullender, M., Hegde, M., Vaimberg, E.W., Donovan, K.F., Smith, I., Tothova, Z., Wilen, C., Orchard, R., et al. (2016). Optimized sgRNA design to maximize activity and minimize off-target effects of CRISPR-Cas9. Nat. Biotechnol. *34*, 184–191.

Emmott, E., and Goodfellow, I. (2014). Identification of protein interaction partners in mammalian cells using SILAC-immunoprecipitation quantitative proteomics. J Vis Exp e51656–e51656.

Emmott, E., de Rougemont, A., Hosmillo, M., Lu, J., Fitzmaurice, T.J., Haas, J., and Goodfellow, I. (2019). Polyprotein processing and intermolecular interactions within the viral replication complex spatially and temporally control norovirus protease activity. J. Biol. Chem. jbc.RA118.006780.

Emmott, E., Sorgeloos, F., Caddy, S.L., Vashist, S., Sosnovtsev, S., Lloyd, R., Heesom, K., Locker, N., and Goodfellow, I. (2017). Norovirus-mediated modification of the translational landscape via virus and host-induced cleavage of translation initiation factors. Mol. Cell Proteomics mcp.M116.062448.

Ettayebi, K., Crawford, S.E., Murakami, K., Broughman, J.R., Karandikar, U., Tenge, V.R., Neill, F.H., Blutt, S.E., Zeng, X.-L., Qu, L., et al. (2016). Replication of human noroviruses in stem cell-derived human enteroids. Science *353*, 1387–1393.

Favre, D., and Trepo, C. (2001). Translational extracts active biologically in vitro obtained from eukaryotic monolayer cells: a versatile method for viral RNA studies. J. Virol. Methods *92*, 177–181.

Firth, A.E., and Brierley, I. (2012). Non-canonical translation in RNA viruses. J. Gen. Virol. *93*, 1385–1409.

Fritzlar, S., Aktepe, T., Chao, Y.-W., McAllaster, M., Wilen, C., White, P., and Mackenzie, J. (2019). Mouse Norovirus infection arrests host cell translation uncoupled from the stress granule-PKR-eIF2α axis. bioRxiv 536052.

Goodfellow, I. (2011). The genome-linked protein VPg of vertebrate viruses — a multifaceted protein. Curr Opin Virol *1*, 355–362.

Goodfellow, I., Chaudhry, Y., Gioldasi, I., Gerondopoulos, A., Natoni, A., Labrie, L., Laliberté, J.-F., and Roberts, L. (2005). Calicivirus translation initiation requires an interaction between VPg and eIF 4 E. EMBO Rep. *6*, 968–972.

Haga, K., Fujimoto, A., Takai-Todaka, R., Miki, M., Doan, Y.H., Murakami, K., Yokoyama, M., Murata, K., Nakanishi, A., and Katayama, K. (2016). Functional receptor molecules CD300lf and CD300ld within the CD300 family enable murine noroviruses to infect cells. Proc. Natl. Acad. Sci. U.S.a. *113*, E6248–E6255.

Hosmillo, M., Chaudhry, Y., Kim, D.-S., Goodfellow, I., and Cho, K.-O. (2014).

Sapovirus translation requires an interaction between VPg and the cap binding protein eIF4E. J Virol *88*, 12213–12221.

Humoud, M.N., Doyle, N., Royall, E., Willcocks, M.M., Sorgeloos, F., van Kuppeveld, F., Roberts, L.O., Goodfellow, I.G., Langereis, M.A., and Locker, N. (2016). Feline Calicivirus Infection Disrupts Assembly of Cytoplasmic Stress Granules and Induces G3BP1 Cleavage. J Virol *90*, 6489–6501.

Hyde, J.L., and Mackenzie, J.M. (2010). Subcellular localization of the MNV-1 ORF1 proteins and their potential roles in the formation of the MNV-1 replication complex. Virology *406*, 138–148.

Hyde, J.L., Sosnovtsev, S.V., Green, K.Y., Wobus, C., Virgin, H.W., and Mackenzie, J.M. (2009). Mouse norovirus replication is associated with virus-induced vesicle clusters originating from membranes derived from the secretory pathway. J Virol *83*, 9709–9719.

Jaafar, Z.A., and Kieft, J.S. (2019). Viral RNA structure-based strategies to manipulate translation. Nat. Rev. Microbiol. *17*, 110–123.

Jones, M.K., Watanabe, M., Zhu, S., Graves, C.L., Keyes, L.R., Grau, K.R., Gonzalez-Hernandez, M.B., Iovine, N.M., Wobus, C.E., Vinjé, J., et al. (2014). Enteric bacteria promote human and mouse norovirus infection of B cells. Science *346*, 755–759.

Karst, S.M., Wobus, C.E., Lay, M., Davidson, J., and Virgin, H.W. (2003). STAT1-dependent innate immunity to a Norwalk-like virus. Science *299*, 1575–1578.

Kedersha, N., Panas, M.D., Achorn, C.A., Lyons, S., Tisdale, S., Hickman, T., Thomas, M., Lieberman, J., McInerney, G.M., Ivanov, P., et al. (2016). G3BP-Caprin1-USP10 complexes mediate stress granule condensation and associate with 40S subunits. J. Cell Biol. *212*, 845–860.

Kim, D.Y., Reynaud, J.M., Rasalouskaya, A., Akhrymuk, I., Mobley, J.A., Frolov, I., and Frolova, E.I. (2016). New World and Old World Alphaviruses Have Evolved to Exploit Different Components of Stress Granules, FXR and G3BP Proteins, for Assembly of Viral Replication Complexes. PLoS Pathog. *12*, e1005810.

Kitano, M., Hosmillo, M., Emmott, E., Lu, J., and Goodfellow, I. (2018). Selection and Characterization of Rupintrivir-Resistant Norwalk Virus Replicon Cells In Vitro. Antimicrob. Agents Chemother. *62*, 725.

Kumar, P., Hellen, C.U.T., and Pestova, T.V. (2016). Toward the mechanism of eIF4F-mediated ribosomal attachment to mammalian capped mRNAs. Genes Dev. *30*, 1573–1588.

Leen, E.N., Sorgeloos, F., Correia, S., Chaudhry, Y., Cannac, F., Pastore, C., Xu, Y., Graham, S.C., Matthews, S.J., Goodfellow, I.G., et al. (2016). A Conserved Interaction between a C-Terminal Motif in Norovirus VPg and the HEAT-1 Domain of eIF4G Is Essential for Translation Initiation. PLoS Pathog. *12*, e1005379.

Li, T.-F., Hosmillo, M., Schwanke, H., Shu, T., Wang, Z., Yin, L., Curry, S.,

Goodfellow, I.G., and Zhou, X. (2018). Human Norovirus NS3 Has RNA Helicase and Chaperoning Activities. J Virol *92*, 312.

López-Manríquez, E., Vashist, S., Ureña, L., Goodfellow, I., Chavez, P., Mora-Heredia, J.E., Cancio-Lonches, C., Garrido, E., and Gutiérrez-Escolano, A.L. (2013). Norovirus Genome Circularisation and Efficient Replication is Facilitated by Binding of PCBP2 and hnRNP A1. J Virol *87*, 11371–11387.

McCormick, C., and Khaperskyy, D.A. (2017). Translation inhibition and stress granules in the antiviral immune response. Nat. Rev. Immunol. *17*, 647–660.

McCune, B.T., Tang, W., Lu, J., Eaglesham, J.B., Thorne, L., Mayer, A.E., Condiff, E., Nice, T.J., Goodfellow, I., Krezel, A.M., et al. (2017). Noroviruses Co-opt the Function of Host Proteins VAPA and VAPB for Replication via a Phenylalanine-Phenylalanine-Acidic-Tract-Motif Mimic in Nonstructural Viral Protein NS1/2. MBio *8*, e00668–17.

Nice, T.J., Strong, D.W., McCune, B.T., Pohl, C.S., and Virgin, H.W. (2012). A single amino acid change in murine norovirus NS1/2 is sufficient for colonic tropism and persistence. J Virol.

Orchard, R.C., Wilen, C.B., Doench, J.G., Baldridge, M.T., McCune, B.T., Lee, Y.-C.J., Lee, S., Pruett-Miller, S.M., Nelson, C.A., Fremont, D.H., et al. (2016). Discovery of a proteinaceous cellular receptor for a norovirus. Science *353*, 933–936.

Panas, M.D., Ahola, T., and McInerney, G.M. (2014). The C-terminal repeat domains of nsP3 from the Old World alphaviruses bind directly to G3BP. J Virol *88*, 5888–5893.

Panas, M.D., Schulte, T., Thaa, B., Sandalova, T., Kedersha, N., Achour, A., and McInerney, G.M. (2015). Viral and cellular proteins containing FGDF motifs bind G3BP to block stress granule formation. PLoS Pathog. *11*, e1004659.

Panas, M.D., Varjak, M., Lulla, A., Eng, K.E., Merits, A., Karlsson Hedestam, G.B., and McInerney, G.M. (2012). Sequestration of G3BP coupled with efficient translation inhibits stress granules in Semliki Forest virus infection. Mol Biol Cell *23*, 4701–4712.

Protter, D.S.W., and Parker, R. (2016). Principles and Properties of Stress Granules. Trends Cell Biol. *26*, 668–679.

Rakotondrafara, A.M., and Hentze, M.W. (2011). An efficient factor-depleted mammalian in vitro translation system. Nat Protoc *6*, 563–571.

Rocha-Pereira, J., Jochmans, D., Dallmeier, K., Leyssen, P., Cunha, R., Costa, I., Nascimento, M.S.J., and Neyts, J. (2012). Inhibition of norovirus replication by the nucleoside analogue 2'-C-methylcytidine. Biochem. Biophys. Res. Commun. *427*, 796–800.

Rocha-Pereira, J., Jochmans, D., Debing, Y., Verbeken, E., Nascimento, M.S.J., and Neyts, J. (2013). The viral polymerase inhibitor 2'-C-methylcytidine inhibits Norwalk

virus replication and protects against norovirus-induced diarrhea and mortality in a mouse model. J Virol *87*, 11798–11805.

Sanjana, N.E., Shalem, O., and Zhang, F. (2014). Improved vectors and genome-wide libraries for CRISPR screening. Nat. Methods *11*, 783–784.

Shannon, P., Markiel, A., Ozier, O., Baliga, N.S., Wang, J.T., Ramage, D., Amin, N., Schwikowski, B., and Ideker, T. (2003). Cytoscape: a software environment for integrated models of biomolecular interaction networks. Genome Res. *13*, 2498–2504.

Thackray, L.B., Wobus, C.E., Chachu, K.A., Liu, B., Alegre, E.R., Henderson, K.S., Kelley, S.T., and Virgin, H.W. (2007). Murine noroviruses comprising a single genogroup exhibit biological diversity despite limited sequence divergence. J Virol *81*, 10460–10473.

Thandapani, P., O'Connor, T.R., Bailey, T.L., and Richard, S. (2013). Defining the RGG/RG motif. Mol. Cell *50*, 613–623.

Thorne, L.G., and Goodfellow, I.G. (2014). Norovirus gene expression and replication. J. Gen. Virol. *95*, 278–291.

Thorne, L., Bailey, D., and Goodfellow, I. (2012). High-Resolution functional profiling of the norovirus genome. J Virol *86*, 11441–11456.

V'kovski, P., Gerber, M., Kelly, J., Pfaender, S., Ebert, N., Braga Lagache, S., Simillion, C., Portmann, J., Stalder, H., Gaschen, V., et al. (2019). Determination of host proteins composing the microenvironment of coronavirus replicase complexes by proximity-labeling. Elife *8*, 25.

van Beek, J., van der Eijk, A.A., Fraaij, P.L.A., Caliskan, K., Cransberg, K., Dalinghaus, M., Hoek, R.A.S., Metselaar, H.J., Roodnat, J., Vennema, H., et al. (2016). Chronic norovirus infection among solid organ recipients in a tertiary care hospital, the Netherlands, 2006-2014. Clin. Microbiol. Infect.

Van, J.D., Ny, A., Conceição-Neto, N., Maes, J., Hosmillo, M., Cuvry, A., Goodfellow, I., de, T.A.N., Verbeken, E., Matthijnssens, J., et al. (2019). A robust human norovirus replication model in zebrafish larvae: Supplementary data file. bioRxiv 528364.

Vashist, S., Ureña, L., and Goodfellow, I. (2012a). Development of a strand specific real-time RT-qPCR assay for the detection and quantitation of murine norovirus RNA. J. Virol. Methods.

Vashist, S., Ureña, L., Chaudhry, Y., and Goodfellow, I. (2012b). Identification of RNA-protein interaction networks involved in the norovirus life cycle. J Virol *86*, 11977–11990.

Villa, N., Do, A., Hershey, J.W.B., and Fraser, C.S. (2013). Human Eukaryotic Initiation Factor 4G (eIF4G) Protein Binds to eIF3c, -d, and -e to Promote mRNA Recruitment to the Ribosome. J. Biol. Chem. *288*, 32932–32940.

Walsh, D., Mathews, M.B., and Mohr, I. (2013). Tinkering with translation: protein synthesis in virus-infected cells. Cold Spring Harb Perspect Biol *5*, a012351–a012351.

White, J.P., Cardenas, A.M., Marissen, W.E., and Lloyd, R.E. (2007). Inhibition of cytoplasmic mRNA stress granule formation by a viral proteinase. Cell Host Microbe *2*, 295–305.

Wobus, C.E., Karst, S.M., Thackray, L.B., Chang, K.-O., Sosnovtsev, S.V., Belliot, G., Krug, A., Mackenzie, J.M., Green, K.Y., and Virgin, H.W. (2004). Replication of Norovirus in cell culture reveals a tropism for dendritic cells and macrophages. PLoS Biol. *2*, e432.

Yunus, M.A., Chung, L.M.W., Chaudhry, Y., Bailey, D., and Goodfellow, I. (2010). Development of an optimized RNA-based murine norovirus reverse genetics system. J. Virol. Methods *169*, 112–118.

(2006). Differential Cleavage of eIF4GI and eIF4GII in Mammalian Cells. 1–12.

Figure 1

A.

```
GV_Murine       -GKKGKNKKGRGRP---GVFRTRGLTDEEYDEFKKRRESRGGKYSIDDYLADREREEEL
GI_Human        GKNKGKTKKGRGRKANYNAFSRRGLNDEEYEESRRLEKEKGGNYSIQEYLEDRQRYEEE
GII_Human       -GKKGKNKTGRGKK--HTAFSSKGLSDEEYDEYKRIREERNGKYSIEEYLQDRDKYYEE
GIV_Human       GKKKGKNKQGRGRK--HTAFSSKGLSDEEYEEFKQLREEKGGKYSIQEYLEDRDRFEEE
                  :***.* ***:     .*  :**.***:** :: .:.:.*:***::** **::  *

GV_Murine       ERD----------EEEAIFGDGFGLKATRRSRKAERAKLGLVSGGDIRARKPIDWNVVG
GI_Human        AEVQAGGDGGIGETEMEIRHRVFFKSKTKRNRQEERRQLGLVTGSEIRKRKPIDWTPPK
GII_Human       AIARATEEDFCEEEEAKIRQRIFRPT--RKQRKEERASLGLVTGSEIRKRNPEDFKPKG
GIV_Human       AYAQACGGDCDDIEISRIRNSIFRPS--RKQRKEERVKLGLVTGSEIRKRKPDDFQPKG
                              *    *  .  ::.*: ** .****:*.:** *:* *:

                    MNV eIF4G binding domain
GV_Murine       SWADDDRQVDYGEKINFE
GI_Human        EWADDDREVDYTEKINFE
GII_Human       LWADDDRSVDYNEKLSFE
GIV_Human       LWADDERTVDYNEKLDFE
                 ****:* *** **: **
```

B.

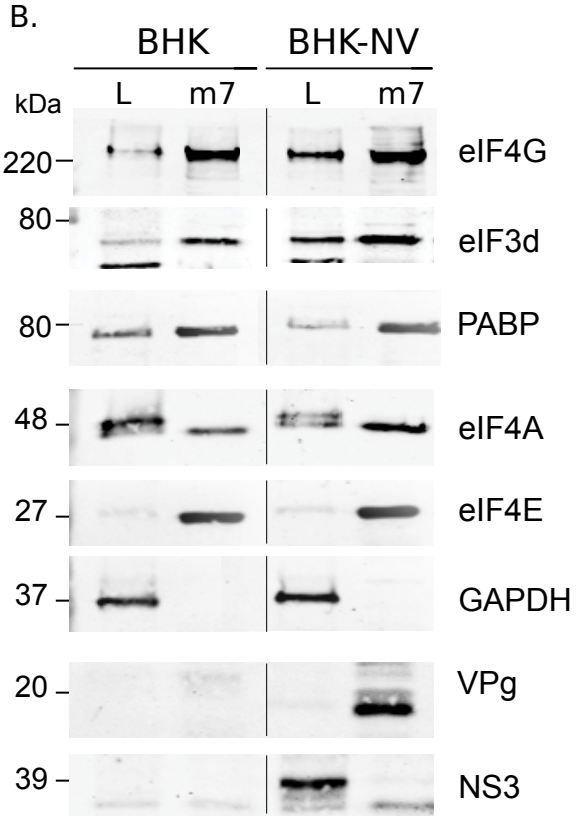

C.

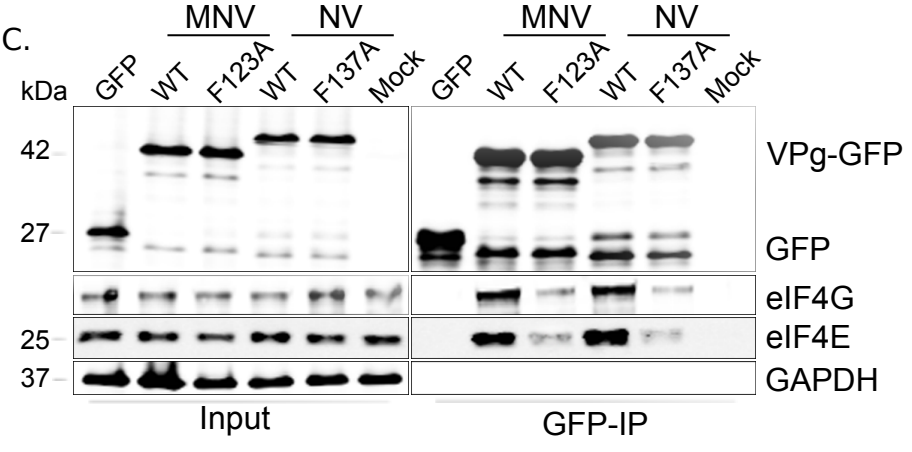

D.

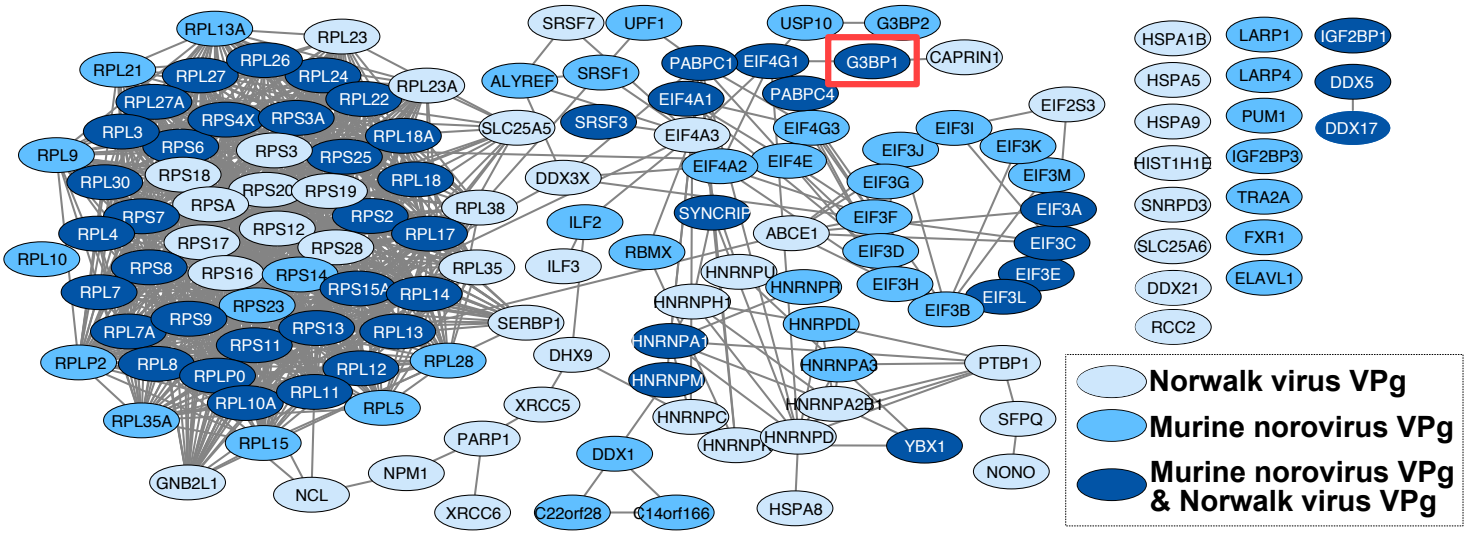

E.

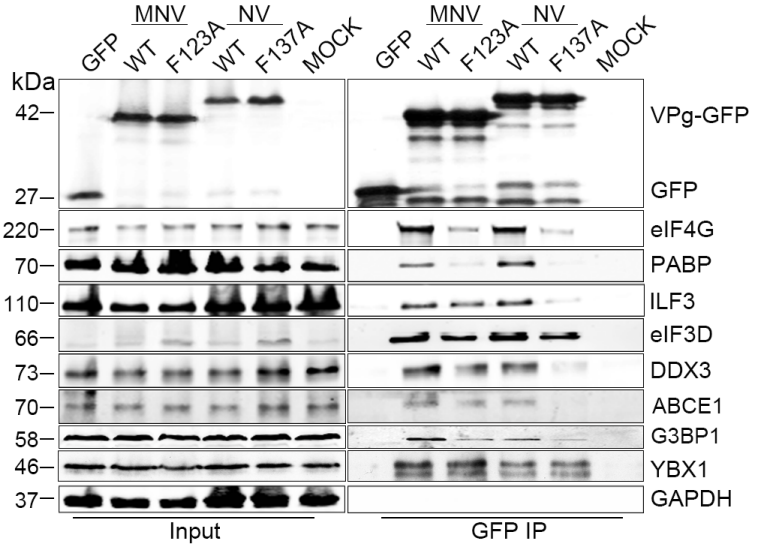

Figure 1-figure supplement 1

A. Host proteins binding to the murine norovirus VPg protein

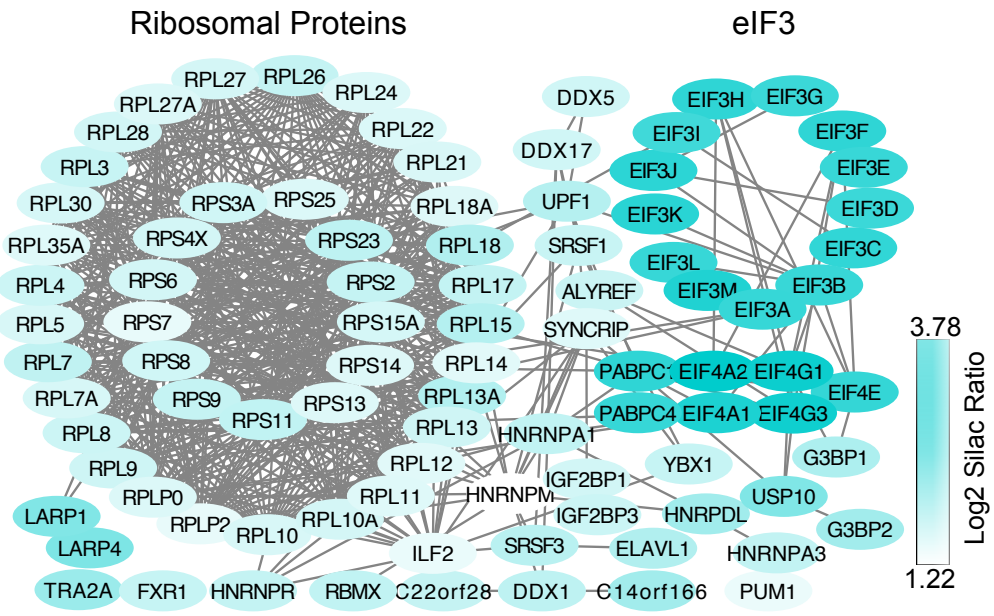

B. Host proteins binding to the Norwalk virus VPg

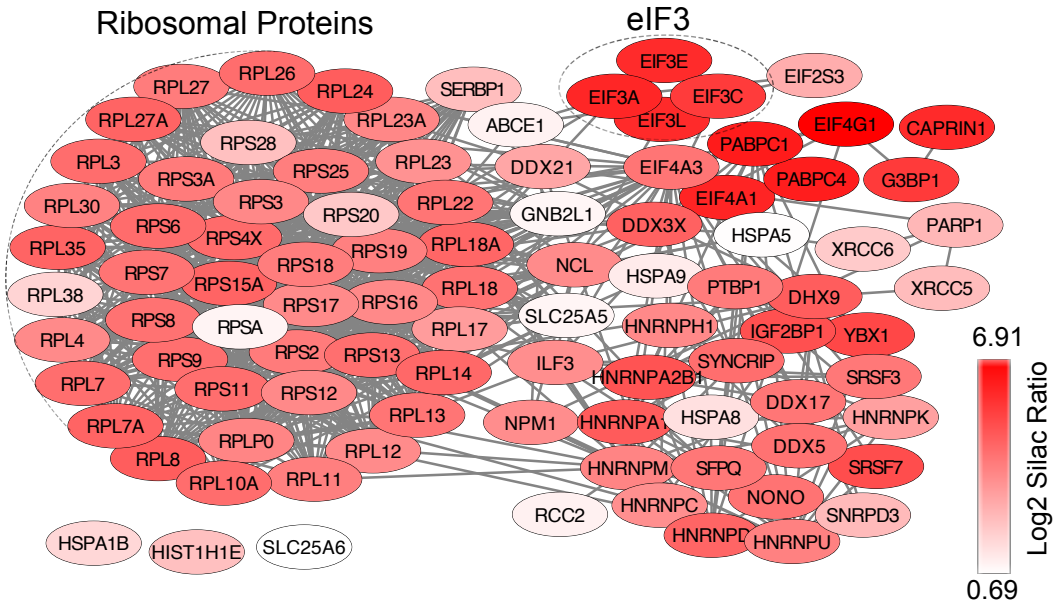

C. Host proteins previously identified as interacting with the MNV VPg protein or the termini of the MNV genoimic RNA

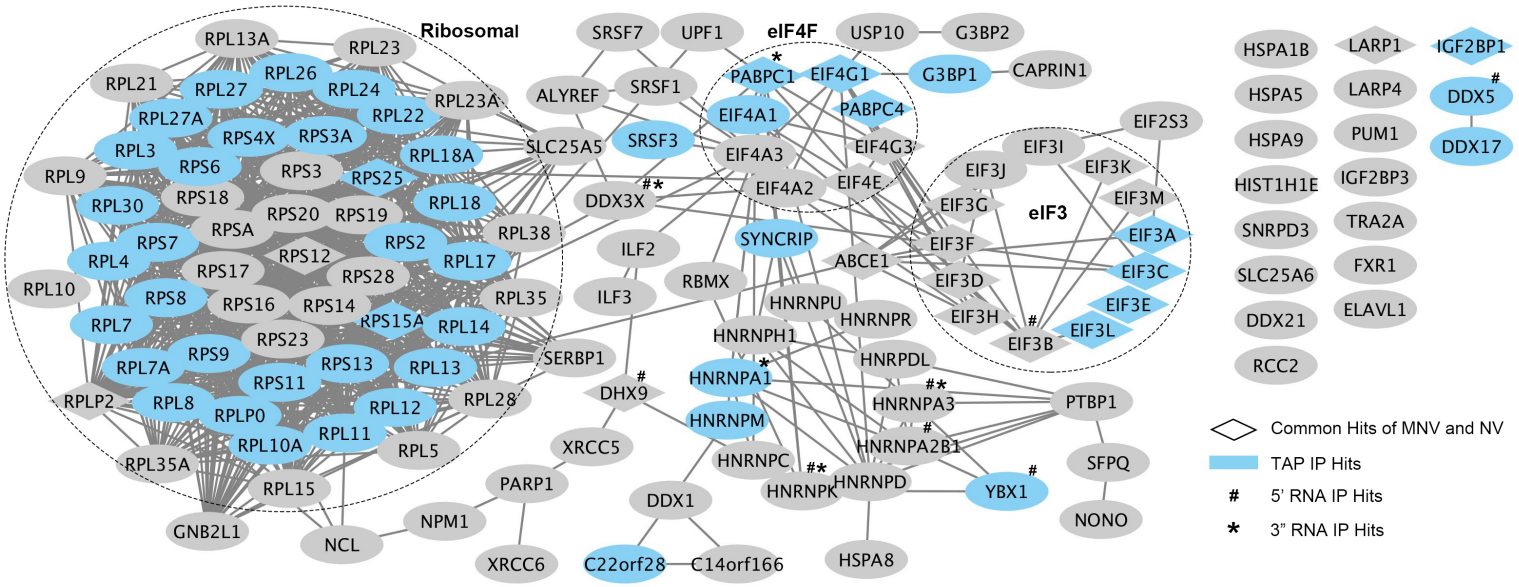

Figure 2

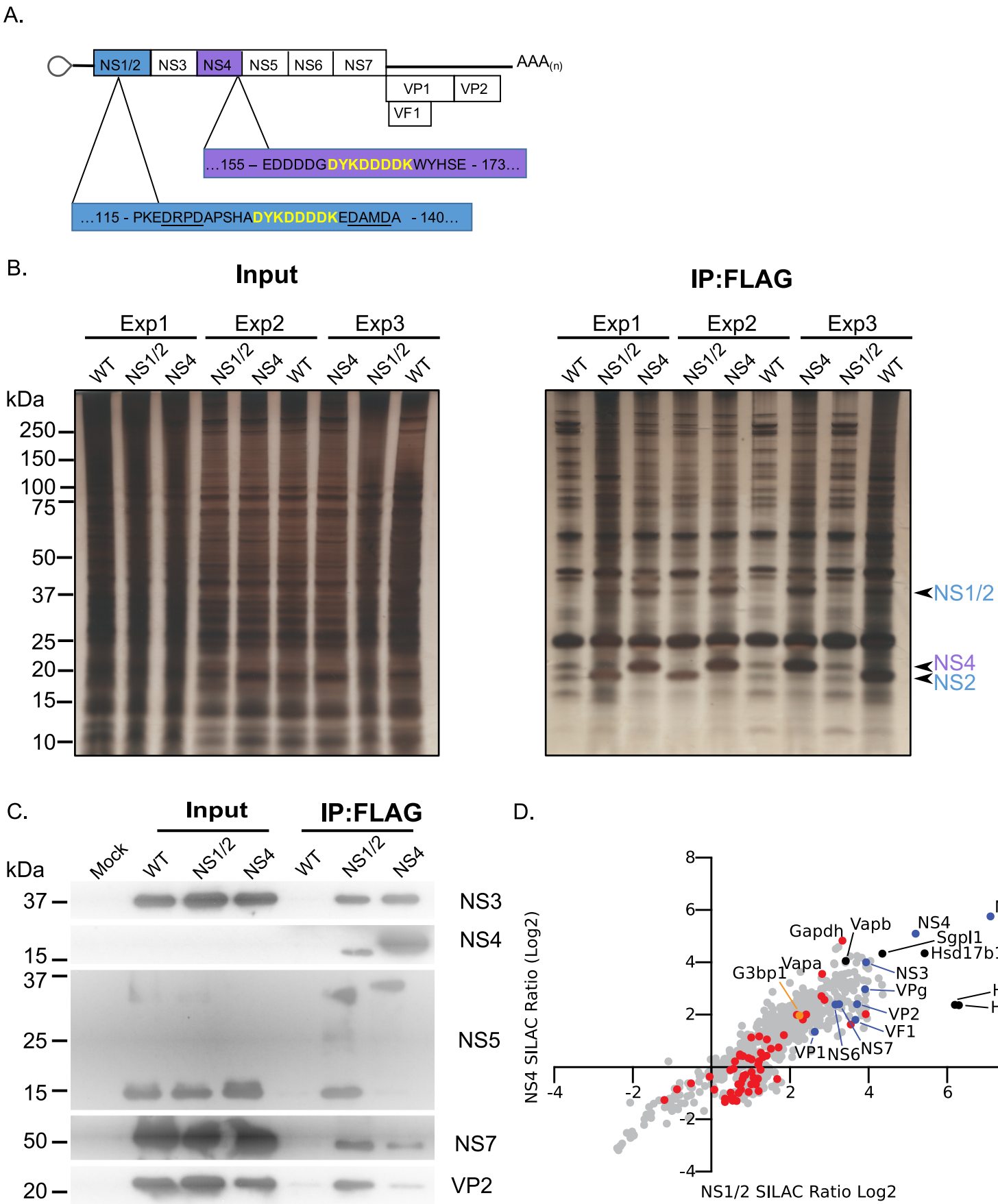
A.
NS1/2
NS3
NS4
NS5
NS6
NS7
AAA(n)
VP1
VP2
VF1
…155 – EDDDDGDYKDDDDKWYHSE - 173…
…115 - PKEDRPDAPSHADYKDDDDKEDAMDA - 140…
B.
Input
IP:FLAG
Exp1
Exp2
Exp3
WT
NS1/2
NS4
kDa
250
150
100
75
50
37
25
20
15
10
NS1/2
NS4
NS2
C.
Input
IP:FLAG
Mock
WT
NS1/2
NS4
kDa
37
15
37
25
15
50
20
NS3
NS4
NS5
NS7
VP2
D.
NS4 SILAC Ratio (Log2)
NS1/2 SILAC Ratio Log2
8
6
4
2
-2
-4
-4
-2
2
4
6
8
Gapdh
Vapb
NS4
NS1/2
Sgpl1
Hsd17b12
Vapa
G3bp1
NS3
VPg
Hadha
Hadhb
VP2
VF1
VP1
NS6
NS7

Figure 2 - figure supplement 1

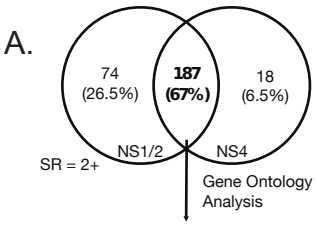

Biological Process	P-value
Protein localization	1.06E-11
Vesicle-mediated transport	7.47E-11
Organelle organization	9.28E-08
Mitochondrion organization	3.49E-07
Exocytosis	1.50E-06
Generation of precursor metabolites and energy	4.92E-06
RNA metabolic process	5.35E-05
Immune response	6.81E-04
Endocytosis	2.38E-03
Fatty acid metabolic process	3.23E-03

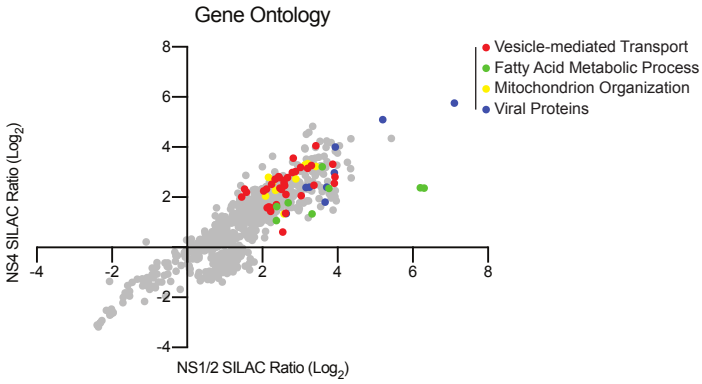

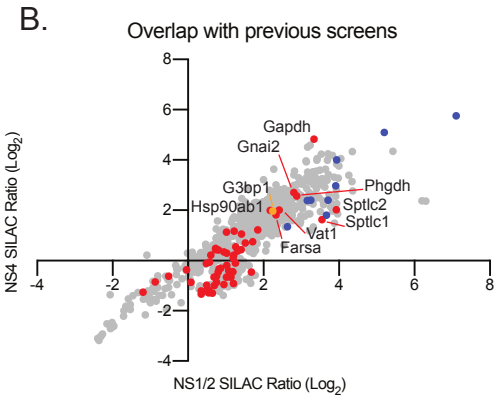

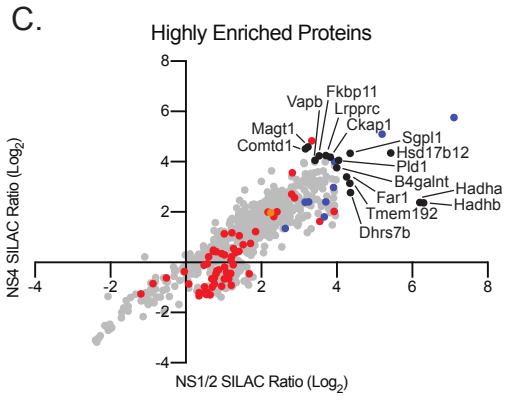

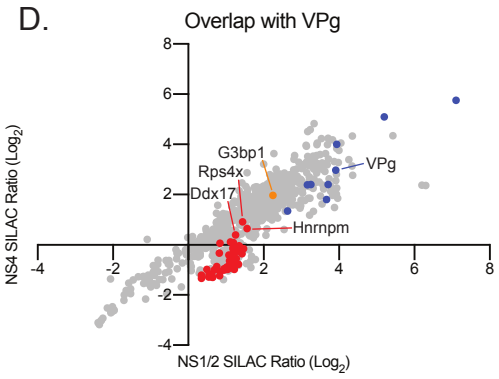

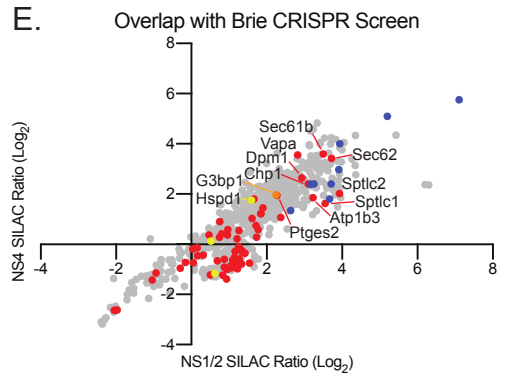

Figure 2 - figure supplement 2

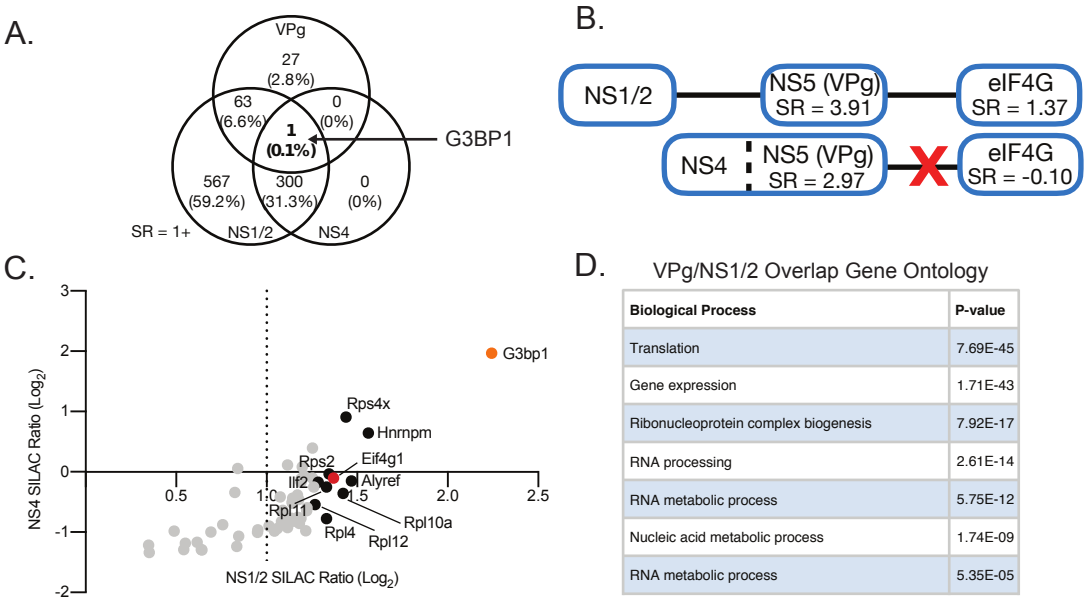

D. VPg/NS1/2 Overlap Gene Ontology

Biological Process	P-value
Translation	7.69E-45
Gene expression	1.71E-43
Ribonucleoprotein complex biogenesis	7.92E-17
RNA processing	2.61E-14
RNA metabolic process	5.75E-12
Nucleic acid metabolic process	1.74E-09
RNA metabolic process	5.35E-05

Figure 3

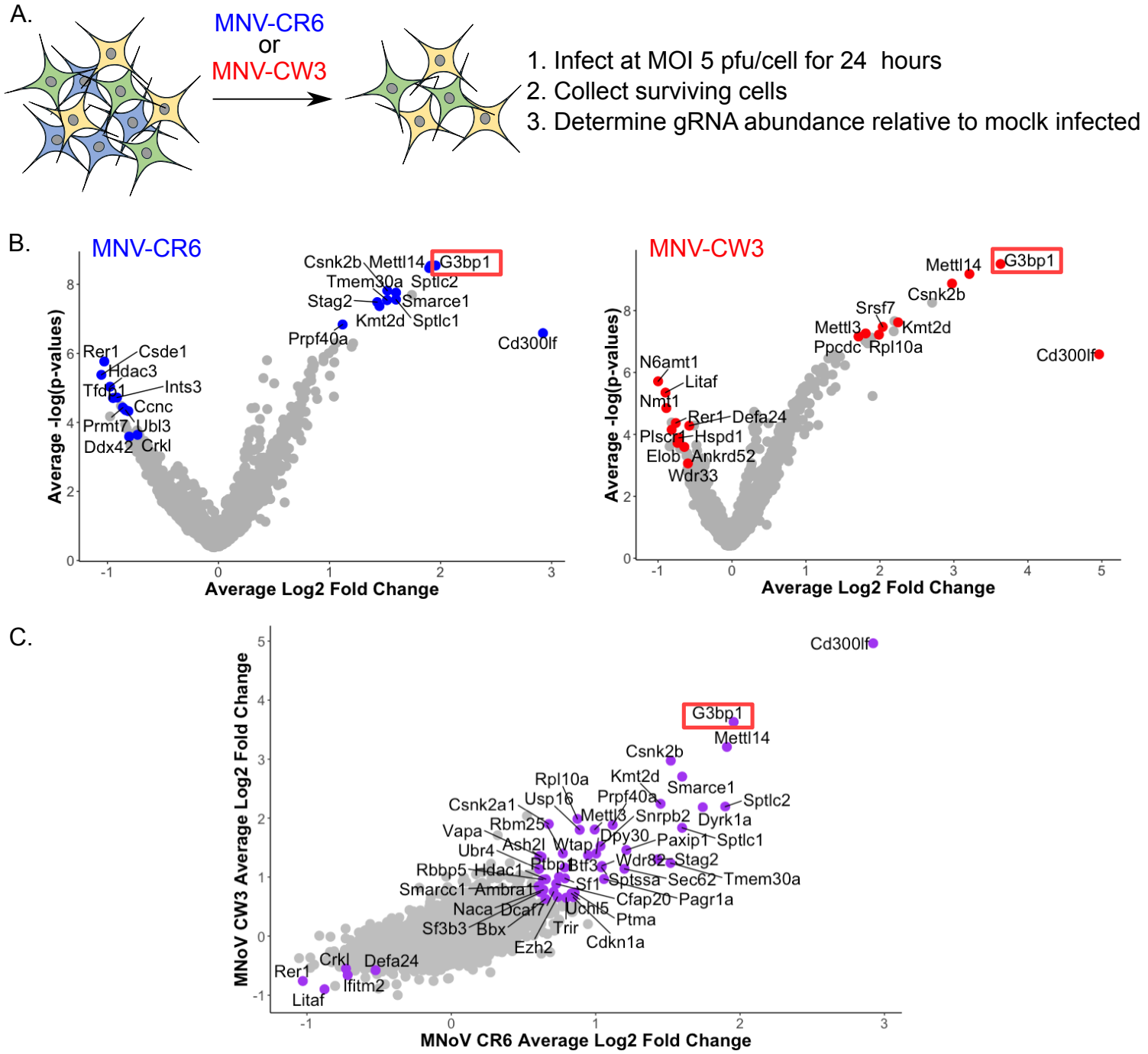
A.
MNV-CR6
or
MNV-CW3
1. Infect at MOI 5 pfu/cell for 24 hours
2. Collect surviving cells
3. Determine gRNA abundance relative to moclk infected
B.
MNV-CR6
Average -log(p-values)
Average Log2 Fold Change
Csnk2b
Mettl14
G3bp1
Tmem30a
Sptlc2
Stag2
Smarce1
Kmt2d
Sptlc1
Prpf40a
Cd300lf
Rer1
Csde1
Hdac3
Ints3
Ccnc
Prmt7
Ubl3
Ddx42
Crkl
MNV-CW3
Average -log(p-values)
Average Log2 Fold Change
Mettl14
G3bp1
Csnk2b
Srsf7
Mettl3
Kmt2d
Ppcdc
Rpl10a
Cd300lf
N6amt1
Litaf
Nmt1
Rer1
Defa24
Plscr1
Hspd1
Elob
Ankrd52
Wdr33
C.
MNoV CW3 Average Log2 Fold Change
MNoV CR6 Average Log2 Fold Change
Cd300lf
G3bp1
Mettl14
Csnk2b
Rpl10a
Kmt2d
Smarce1
Csnk2a1
Usp16
Prpf40a
Sptlc2
Mettl3
Snrpb2
Dyrk1a
Rbm25
Vapa
Dpy30
Paxip1
Sptlc1
Ash2l
Wtap
Ubr4
Rbbp5
Hdac1
Rbbp7
Btf3
Wdr82
Stag2
Smarcc1
Ambra1
Sf1
Sptssa
Sec62
Tmem30a
Cfap20
Pagr1
Naca
Dcaf7
Uchl5
Ptma
Sf3b3
Bbx
Trir
Cdkn1a
Ezh2
Crkl
Defa24
Rer1
Ifitm2
Litaf

Figure 4

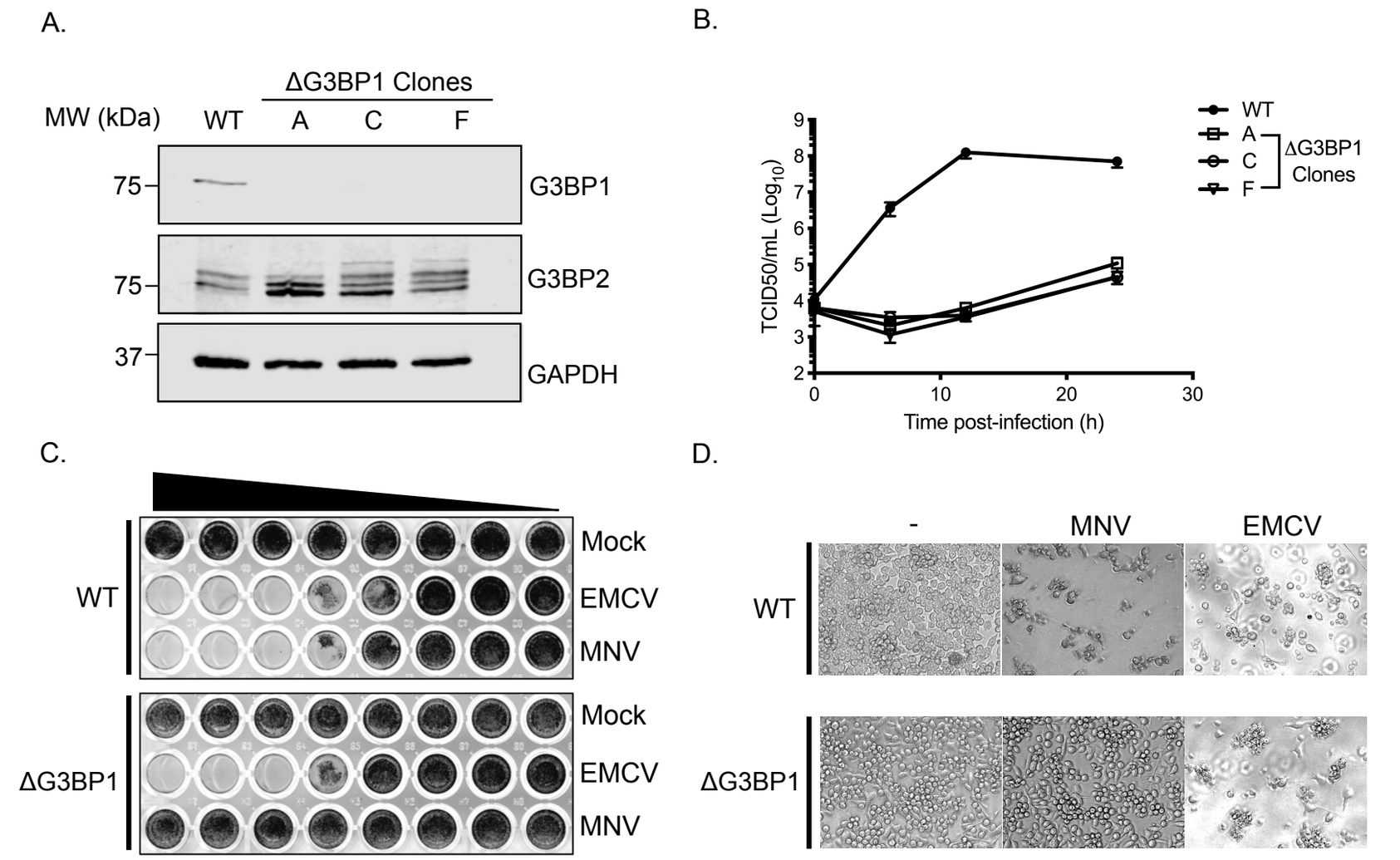
A.
ΔG3BP1 Clones
MW (kDa)
WT
A
C
F
75
G3BP1
75
G3BP2
37
GAPDH
B.
WT
A
C
F
ΔG3BP1 Clones
TCID50/mL (Log10)
Time post-infection (h)
C.
WT
ΔG3BP1
Mock
EMCV
MNV
D.
-
MNV
EMCV
WT
ΔG3BP1

Figure 5

A.

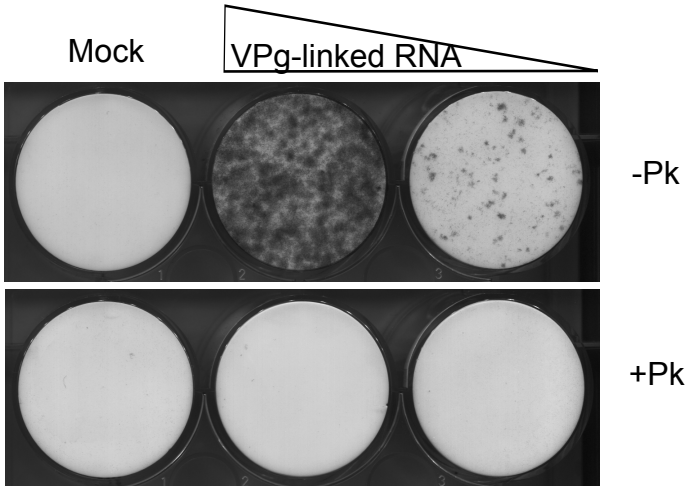

B.

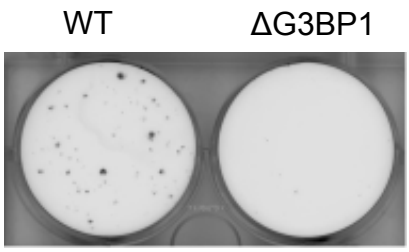

C.

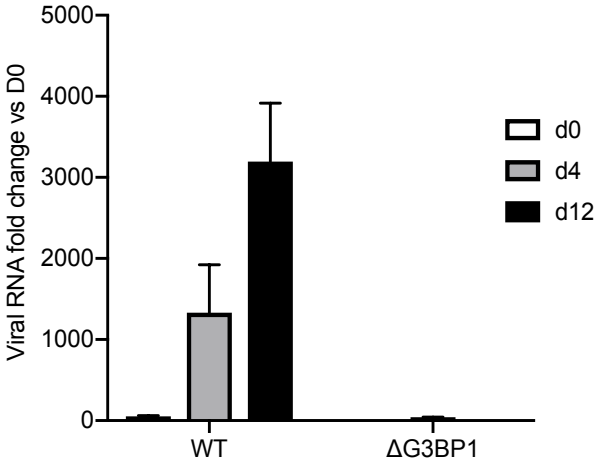

D.

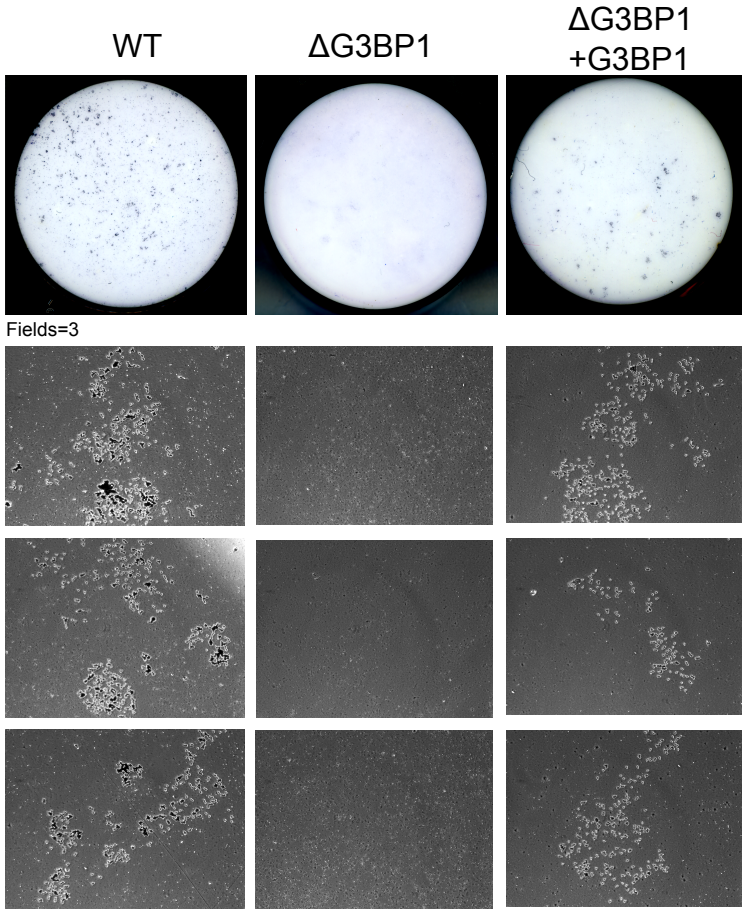

Figure 6

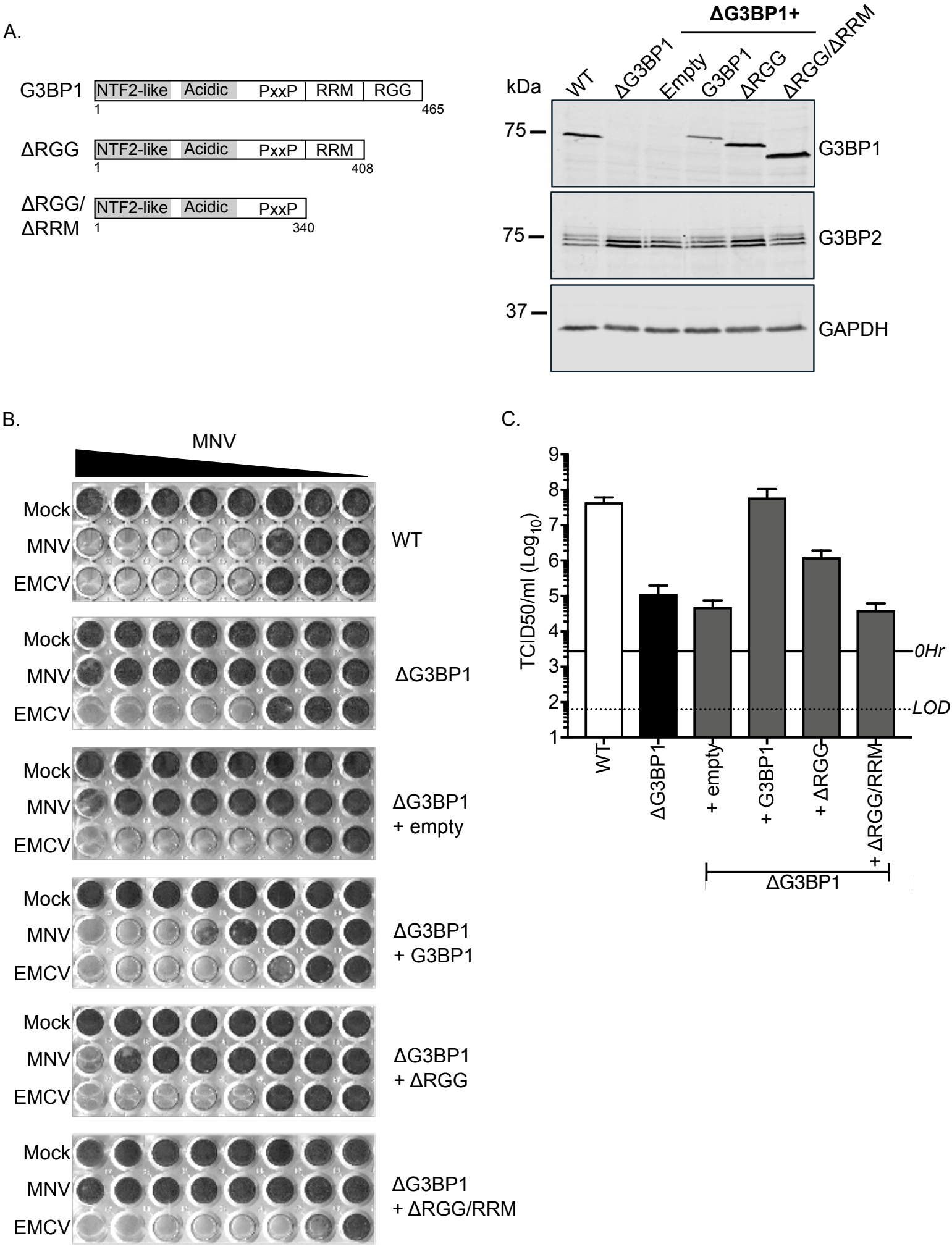
A.
G3BP1
NTF2-like
Acidic
PxxP
RRM
RGG
1
465
ΔRGG
NTF2-like
Acidic
PxxP
RRM
1
408
ΔRGG/
ΔRRM
NTF2-like
Acidic
PxxP
1
340
ΔG3BP1+
kDa
WT
ΔG3BP1
Empty
G3BP1
ΔRGG
ΔRGG/ΔRRM
75
G3BP1
75
G3BP2
37
GAPDH
B.
MNV
Mock
MNV
EMCV
WT
ΔG3BP1
ΔG3BP1
+ empty
ΔG3BP1
+ G3BP1
ΔG3BP1
+ ΔRGG
ΔG3BP1
+ ΔRGG/RRM
C.
TCID50/ml (Log10)
9
8
7
6
5
4
3
2
1
0Hr
LOD
WT
ΔG3BP1
+ empty
+ G3BP1
+ ΔRGG
+ ΔRGG/RRM
ΔG3BP1

Figure 7

A.

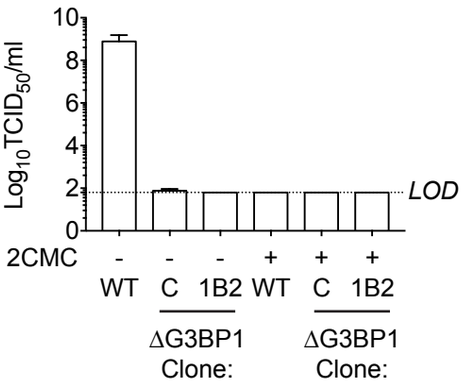

B.

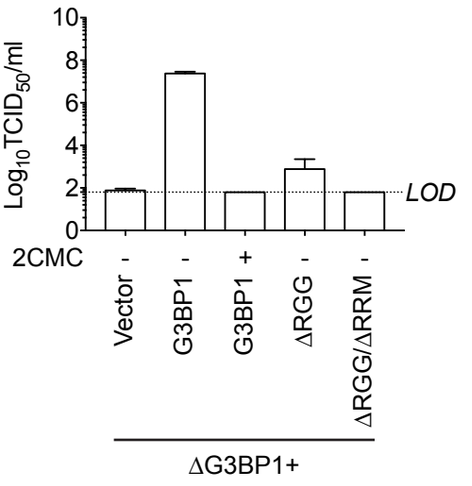

C.

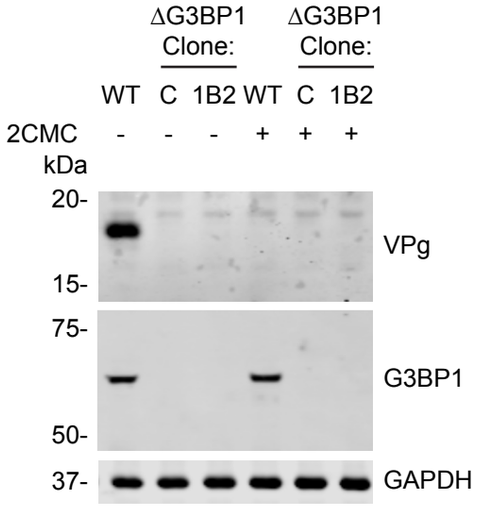

D.

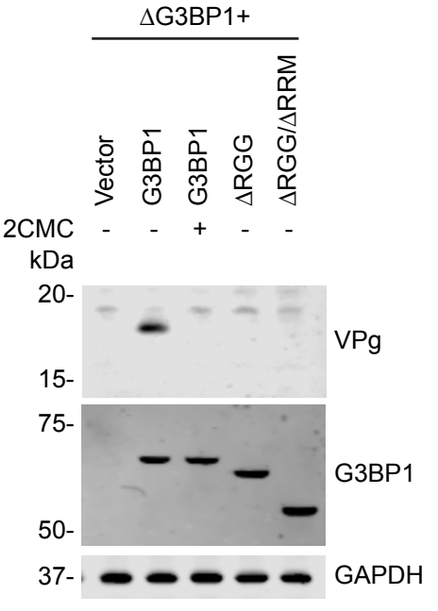

Figure 8

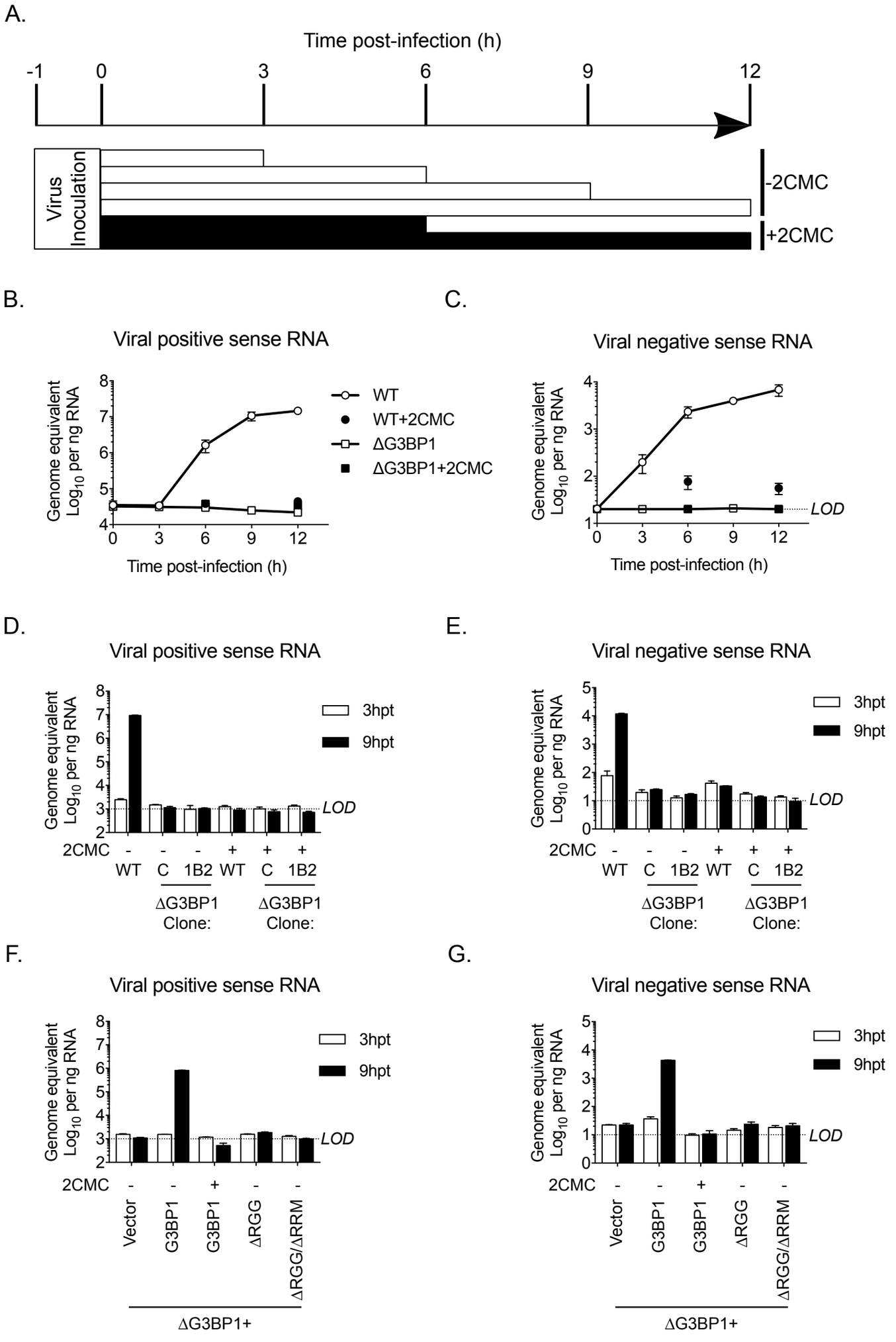
A.
Time post-infection (h)
-1
0
3
6
9
12
Virus Inoculation
-2CMC
+2CMC
B.
Viral positive sense RNA
Genome equivalent Log10 per ng RNA
WT
WT+2CMC
ΔG3BP1
ΔG3BP1+2CMC
Time post-infection (h)
C.
Viral negative sense RNA
Genome equivalent Log10 per ng RNA
LOD
Time post-infection (h)
D.
Viral positive sense RNA
Genome equivalent Log10 per ng RNA
3hpt
9hpt
LOD
2CMC
WT C 1B2 WT C 1B2
ΔG3BP1 Clone:
ΔG3BP1 Clone:
E.
Viral negative sense RNA
Genome equivalent Log10 per ng RNA
3hpt
9hpt
LOD
2CMC
WT C 1B2 WT C 1B2
ΔG3BP1 Clone:
ΔG3BP1 Clone:
F.
Viral positive sense RNA
Genome equivalent Log10 per ng RNA
3hpt
9hpt
LOD
2CMC
Vector
G3BP1
G3BP1
ΔRGG
ΔRGG/ΔRRM
ΔG3BP1+
G.
Viral negative sense RNA
Genome equivalent Log10 per ng RNA
3hpt
9hpt
LOD
2CMC
Vector
G3BP1
G3BP1
ΔRGG
ΔRGG/ΔRRM
ΔG3BP1+

Figure 9

A.

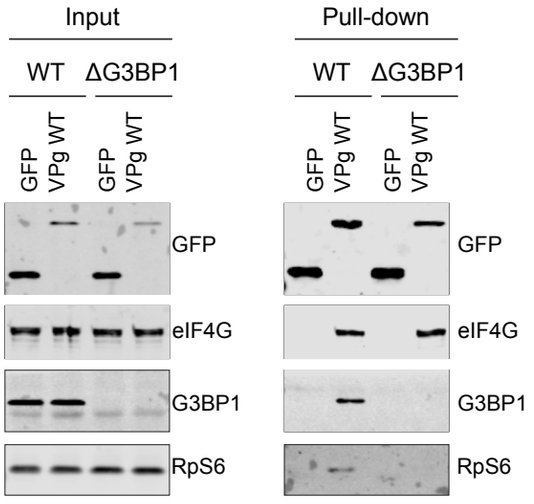
Input
Pull-down
WT
ΔG3BP1
WT
ΔG3BP1
GFP
VPg WT
GFP
VPg WT
GFP
VPg WT
GFP
VPg WT
GFP
eIF4G
G3BP1
RpS6
GFP
eIF4G
G3BP1
RpS6

B.

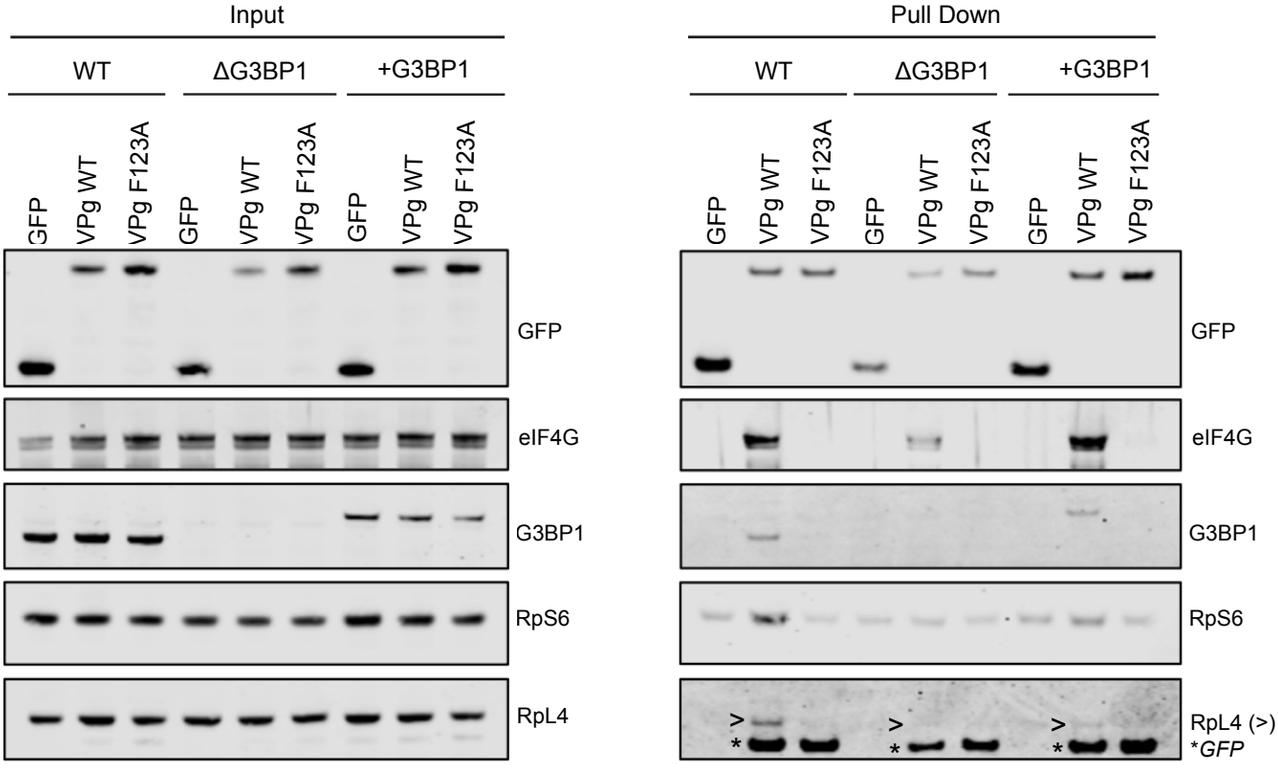
Input
Pull Down
WT
ΔG3BP1
+G3BP1
WT
ΔG3BP1
+G3BP1
GFP
VPg WT
VPg F123A
GFP
VPg WT
VPg F123A
GFP
VPg WT
VPg F123A
GFP
VPg WT
VPg F123A
GFP
VPg WT
VPg F123A
GFP
VPg WT
VPg F123A
GFP
eIF4G
G3BP1
RpS6
RpL4
GFP
eIF4G
G3BP1
RpS6
RpL4 (>)
*GFP

C.

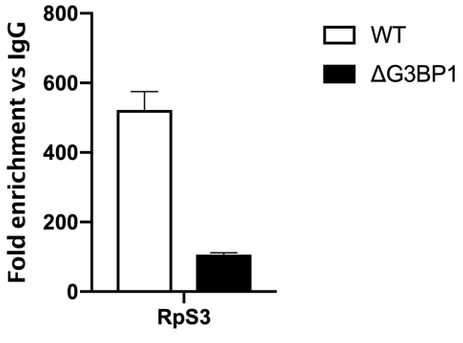
Fold enrichment vs IgG
800
600
400
200
0
RpS3
WT
ΔG3BP1

Figure 9 - figure supplement 1

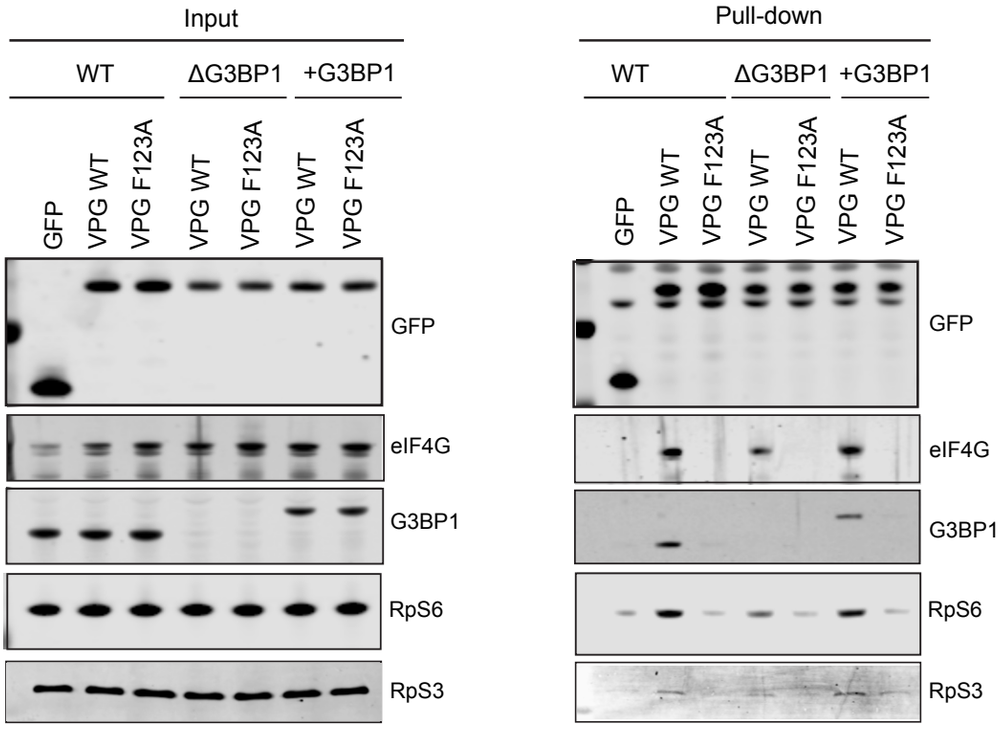

Figure 10

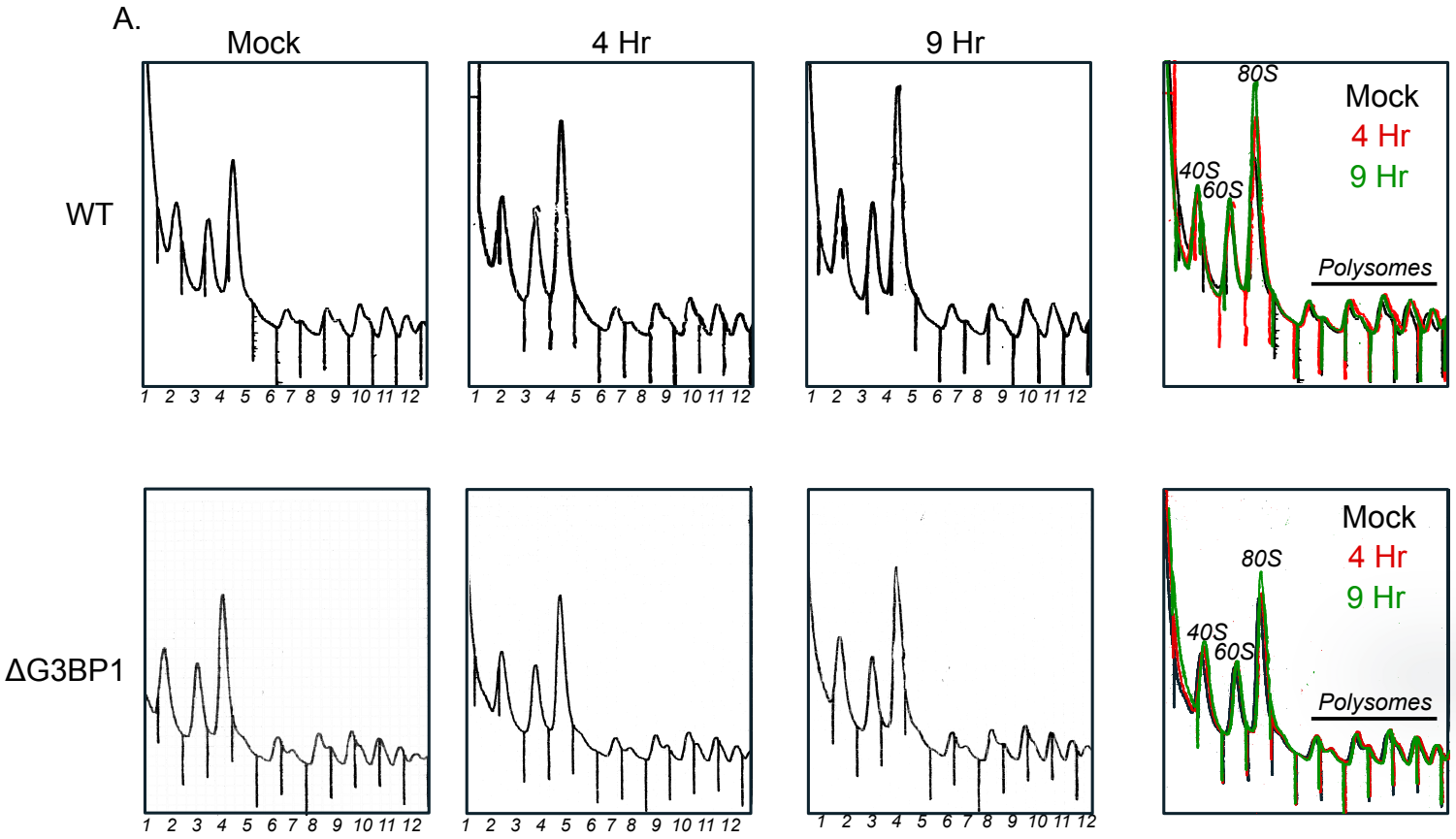
A.
Mock
4 Hr
9 Hr
WT
ΔG3BP1
80S
40S
60S
Polysomes
1 2 3 4 5 6 7 8 9 10 11 12

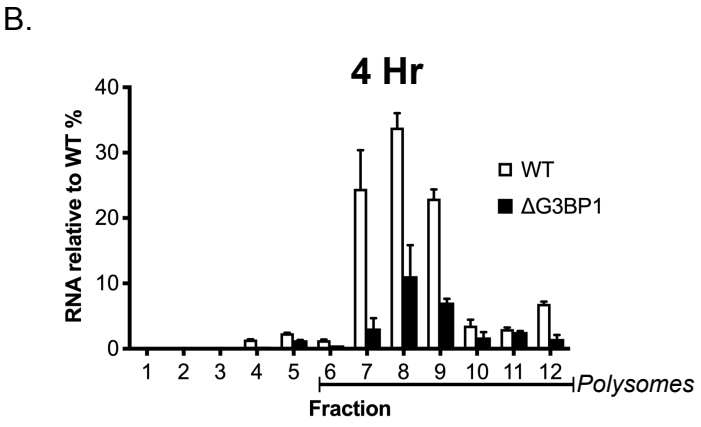
B.
4 Hr
9 Hr
RNA relative to WT %
WT
ΔG3BP1
Fraction
Polysomes

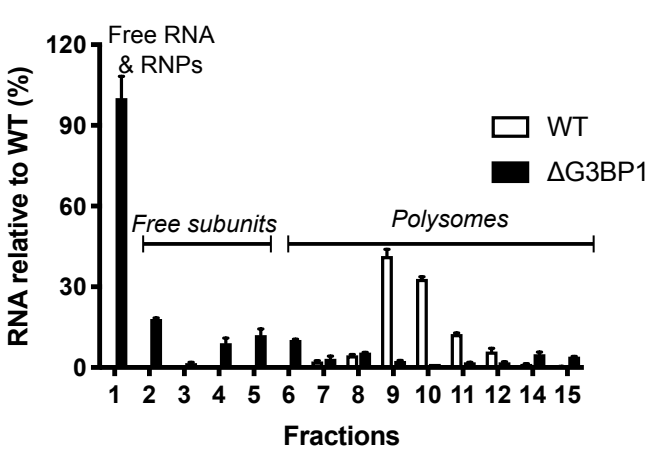
C.
Free RNA
& RNPs
RNA relative to WT (%)
WT
ΔG3BP1
Free subunits
Polysomes
Fractions

Figure 11

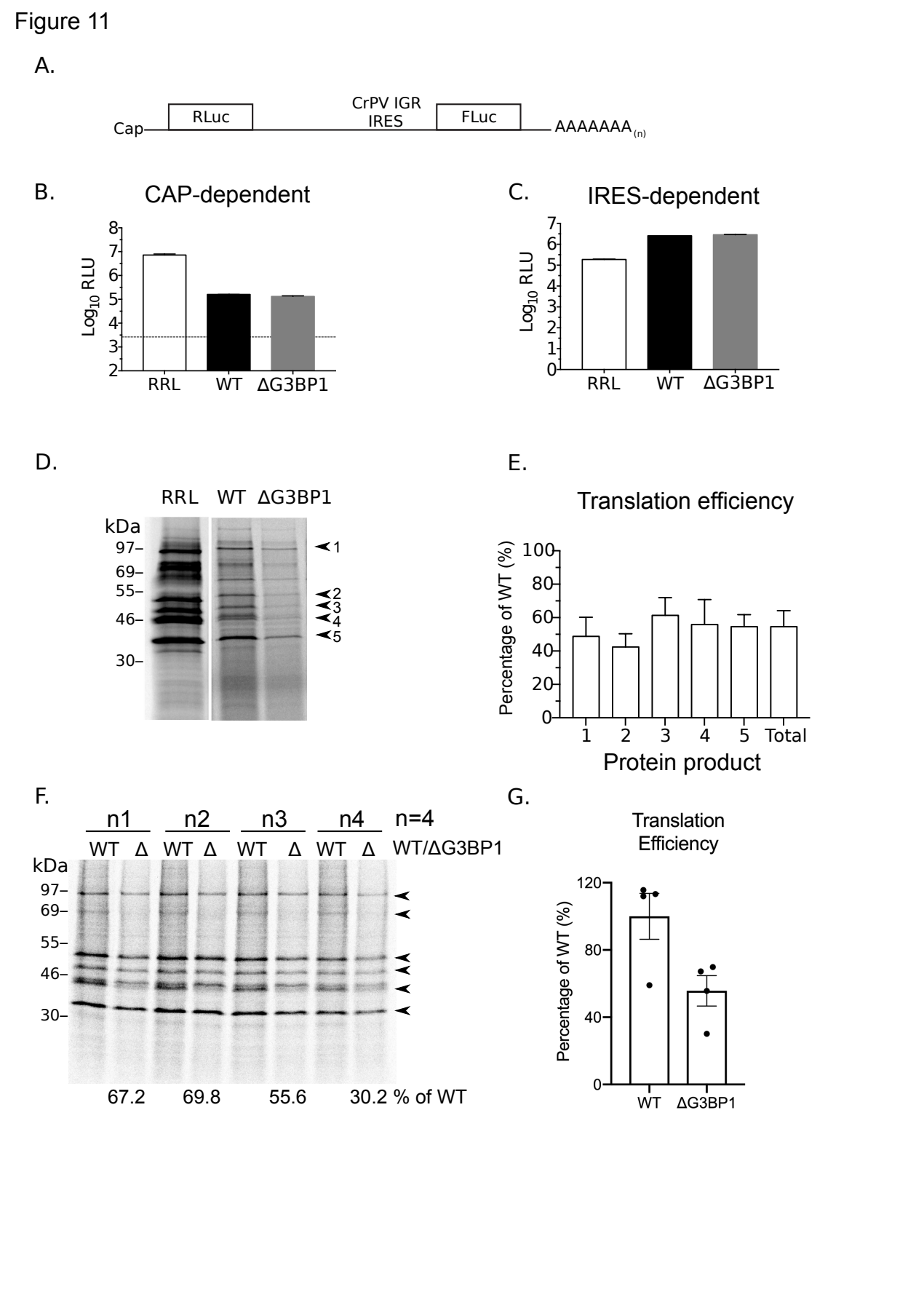
A.
Cap
RLuc
CrPV IGR IRES
FLuc
AAAAAAA(n)
B.
CAP-dependent
Log10 RLU
RRL
WT
ΔG3BP1
C.
IRES-dependent
Log10 RLU
RRL
WT
ΔG3BP1
D.
RRL
WT
ΔG3BP1
kDa
97–
69–
55–
46–
30–
1
2
3
4
5
E.
Translation efficiency
Percentage of WT (%)
1
2
3
4
5
Total
Protein product
F.
n1
n2
n3
n4
n=4
WT
Δ
WT/ΔG3BP1
kDa
97–
69–
55–
46–
30–
67.2
69.8
55.6
30.2 % of WT
G.
Translation Efficiency
Percentage of WT (%)
WT
ΔG3BP1

Figure 11 - figure supplement 1